eLIFE elifesciences.org

RESEARCH ARTICLE

Early structural and functional plasticity alterations in a susceptibility period of DYT1 dystonia mouse striatum

Marta Maltese[1,2], Jennifer Stanic[3], Annalisa Tassone[1,2], Giuseppe Sciamanna[1,2], Giulia Ponterio[1,2], Valentina Vanni[1,2], Giuseppina Martella[1,2], Paola Imbriani[1,2], Paola Bonsi[2], Nicola Biagio Mercuri[1,2], Fabrizio Gardoni[3†], Antonio Pisani[1,2†*]

[1]Department of Systems Medicine, University of Rome Tor Vergata, Rome, Italy; [2]IRCCS Fondazione Santa Lucia, Rome, Italy; [3]Department of Pharmacology, University of Milan, Milan, Italy

Abstract The onset of abnormal movements in DYT1 dystonia is between childhood and adolescence, although it is unclear why clinical manifestations appear during this developmental period. Plasticity at corticostriatal synapses is critically involved in motor memory. In the *Tor1a*$^{+/\Delta gag}$ DYT1 dystonia mouse model, long-term potentiation (LTP) appeared prematurely in a critical developmental window in striatal spiny neurons (SPNs), while long-term depression (LTD) was never recorded. Analysis of dendritic spines showed an increase of both spine width and mature mushroom spines in *Tor1a*$^{+/\Delta gag}$ neurons, paralleled by an enhanced AMPA receptor (AMPAR) accumulation. BDNF regulates AMPAR expression during development. Accordingly, both proBDNF and BDNF levels were significantly higher in *Tor1a*$^{+/\Delta gag}$ mice. Consistently, antagonism of BDNF rescued synaptic plasticity deficits and AMPA currents. Our findings demonstrate that early loss of functional and structural synaptic homeostasis represents a unique endophenotypic trait during striatal maturation, promoting the appearance of clinical manifestations in mutation carriers.

DOI: https://doi.org/10.7554/eLife.33331.001

***For correspondence:** pisani@uniroma2.it

[†]These authors contributed equally to this work

Competing interests: The authors declare that no competing interests exist.

Funding: See page 18

Received: 03 November 2017
Accepted: 02 March 2018
Published: 05 March 2018

Reviewing editor: Christian Rosenmund, Charité-Universitätsmedizin Berlin, Germany

Introduction

Early-onset generalized torsion dystonia (DYT1) is an autosomal dominant movement disorder, commonly caused by a GAG base-pair deletion in the TOR1A gene coding for torsinA protein, without gross brain structural defects or other detectable neuropathology (***Ozelius et al., 1997***; ***Ledoux et al., 2013***). Intriguingly, only 30–40% of DYT1 mutation carriers develop dystonia, typically in childhood-early adolescence (***Bressman et al., 2000***). However, what triggers the clinical onset of symptoms is currently unknown, although the presence of a critical developmental period of susceptibility is highly probable, since mutation carriers that do not develop symptoms in that time-window remain unaffected for their entire life (***Pappas et al., 2014***).

Plasticity changes include functional and structural synaptic specialization, leading to experience-dependent acquisition of motor skills. However, genetic or acquired alterations may lead to maladaptive plasticity changes. Accordingly, human studies indicate neural processing and synaptic plasticity alterations as major determinants in dystonia pathophysiology (***Quartarone and Hallett, 2013***). A significantly enhanced responsiveness to plasticity protocols has been reported in dystonic patients (***Edwards et al., 2006***; ***Weise et al., 2006***; ***Quartarone et al., 2009***). Moreover, patterns of impaired motor learning have been described even in clinically unaffected DYT1 mutation carriers (***Ghilardi et al., 2003***), further supporting the notion that aberrant plasticity represents a unique endophenotype in dystonia.

Of note, an impairment of striatal plasticity has been demonstrated in a number of different DYT1 models, including transgenic mice and rats overexpressing mutant torsinA (**Martella et al., 2009**; **Grundmann et al., 2012**), knock-in mice heterozygous for Δgag-torsinA (**Dang et al., 2012**; **Martella et al., 2014**; **Rittiner et al., 2016**), revealing an impressive similarity with studies of synaptic plasticity in human dystonia. Collectively, these observations support the hypothesis that DYT1 dystonia is a complex neurodevelopmental disorder of abnormal neurochemistry, wiring, and physiology (**Goodchild et al., 2013**; **Pappas et al., 2014**).

However, these alterations were observed in adult rodents, and to date, a relationship between age and corticostriatal plasticity in dystonia is still lacking. Furthermore, the question as to whether functional and structural plasticity abnormalities occur early in life or later as adaptive changes remains unknown. We report structural and functional abnormalities occurring in a defined postnatal time-window in *Tor1a*$^{+/\Delta gag}$ mice, indicative of a 'premature' and abnormal functional and structural plasticity, which is paralleled by a time-dependent increase in both BDNF levels and AMPAR-mediated currents.

Our findings reveal molecular, functional and structural changes in DYT1 striatal spiny projection neurons (SPNs), emphasizing the link between abnormal plasticity and dystonia. Understanding the key stages at which synaptic circuits are affected could suggest new routes to prevent or treat the disorder.

Results

The critical period for symptom onset in DYT1 dystonia matches a time-window of postnatal life when motor memories are shaped by activity-dependent changes in the striatum. Thus, in order to characterize plasticity changes in the early adolescence, *Tor1a*$^{+/\Delta gag}$ mice were recorded from postnatal day P15 to P35, in good agreement with the approximate life phase equivalencies between humans and mice, predicting that ~4 weeks of mouse age correspond to ~14 years in humans (**Flurkey et al., 2007**).

Electrophysiological characterization of SPNs

Properties of adult *Tor1a*$^{+/\Delta gag}$ SPNs have been extensively characterized (**Maltese et al., 2014**; **Martella et al., 2014**). Here, we focused on intrinsic and synaptic properties of juvenile *Tor1a*$^{+/\Delta gag}$ neurons. SPNs recorded at P26 from both *Tor1a*$^{+/+}$ and *Tor1a*$^{+/\Delta gag}$ mice did not display firing activity at rest and exhibited no significant differences in their intrinsic membrane properties (data not shown). Depolarizing and hyperpolarizing current steps caused tonic action potential discharge and strong inward membrane rectification (**Figure 1A**). Short ISI (25–50 ms) of paired synaptic stimulation induced PPF in both genotypes (**Figure 1B**; $p<0.05$). At longer ISI (100–1000 ms), PPF was not observed in juvenile *Tor1a*$^{+/+}$ and *Tor1a*$^{+/\Delta gag}$ mice (**Figure 1B**; $p>0.05$). To explore potential differences in neurotransmitter release, we recorded spontaneous glutamate- and GABA-mediated currents in P26 SPNs from both *Tor1a*$^{+/+}$ and *Tor1a*$^{+/\Delta gag}$ mice. Glutamatergic sEPSCs did not differ between genotypes (**Figure 1C**; $p>0.05$). However, we found a significant increase in the amplitude, but not in the frequency, of mEPSCs recorded from *Tor1a*$^{+/\Delta gag}$ mice compared to wild types (**Figure 1D**; $p<0.05$). Conversely, GABAergic sIPSCs were unchanged in *Tor1a*$^{+/\Delta gag}$ with respect to *Tor1a*$^{+/+}$ littermates (**Figure 1E**; $p>0.05$). Also, mIPSCs were similar in both genotypes (**Figure 1F**; $p>0.05$).

Premature expression of corticostriatal synaptic plasticity

We previously demonstrated a marked impairment of bidirectional synaptic plasticity in adult (P60-P75) *Tor1a*$^{+/\Delta gag}$ striatum (**Martella et al., 2014**). However, it remains unclear whether these patterns of abnormal plasticity are core pathologic features in an early developmental period, or occur later as maladaptive changes. Thus, we performed a detailed characterization of LTD and LTP from P15 to P35 in *Tor1a*$^{+/+}$ and *Tor1a*$^{+/\Delta gag}$ mice. In *Tor1a*$^{+/+}$ SPNs, HFS failed to induce LTD from P15 to P27 (**Figure 2A**; $p>0.05$). Conversely, the HFS protocol elicited a robust LTD from P28 to P35 (**Figure 2A**; 59.63 ± 2.63% of control; $p<0.05$). Surprisingly, in slices from *Tor1a*$^{+/\Delta gag}$ mice, HFS stimulation failed to cause a synaptic depression, independently from the postnatal day of recording (**Figure 2B**; $p>0.05$).

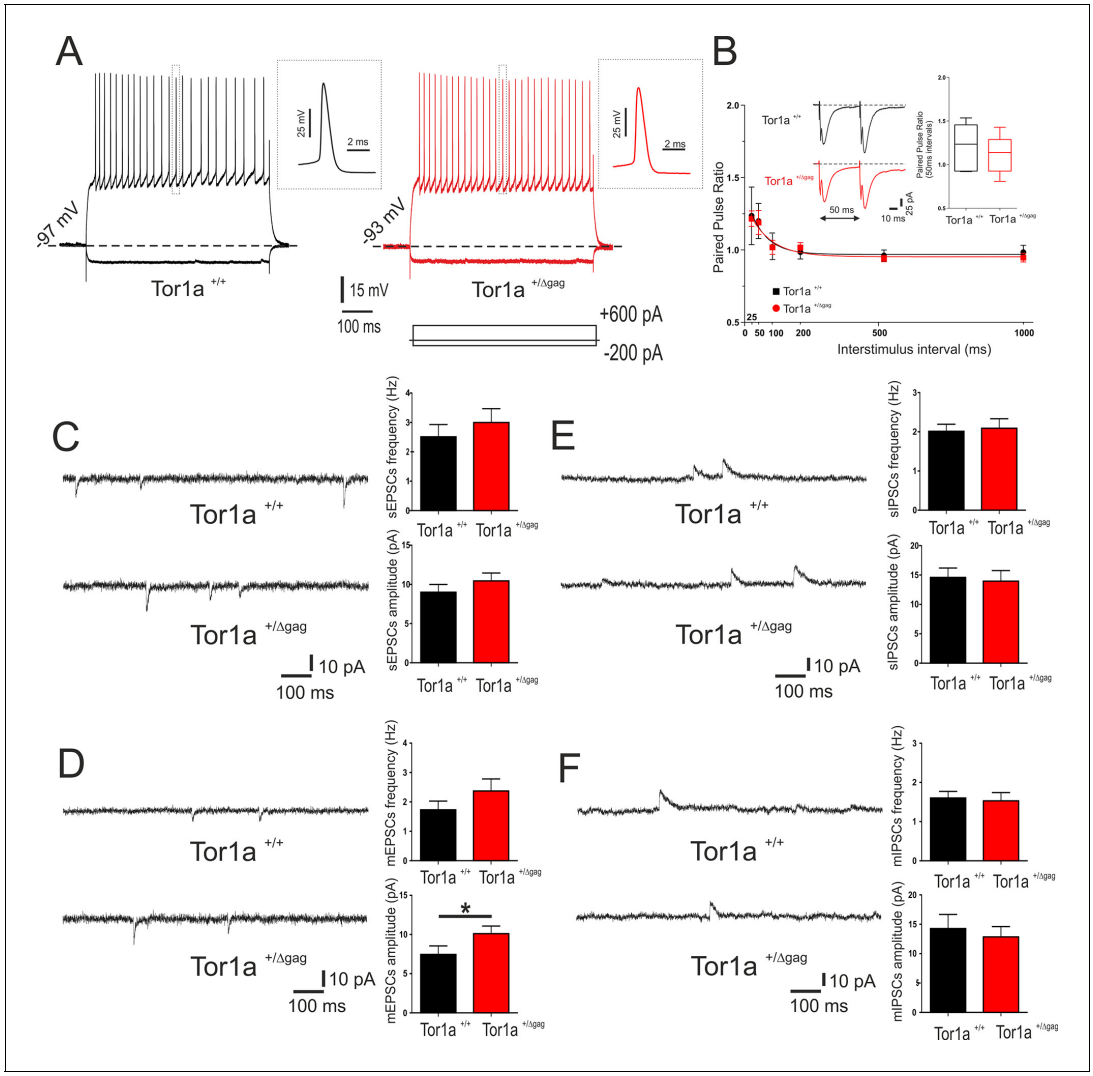

Figure 1. Electrophysiological and synaptic properties of striatal SPNs. (**A**) Superimposed traces showing voltage responses to both depolarizing (+600 pA) and hyperpolarizing (−200 pA) current steps in SPNs recorded from P26 *Tor1a*$^{+/+}$ (black) and *Tor1a*$^{+/\Delta gag}$ (red) mice. The insets display single action potentials (amplitude: *Tor1a*$^{+/+}$69.62 ± 1.14 mV, N = 11, n = 11; *Tor1a*$^{+/\Delta gag}$66.65 ± 1.68 mV, N = 8, n = 11; Student's t test p>0.05). (**B**) Summary plot of paired-pulse ratio values showing similar facilitation in both genotypes. Each data point represents mean ± SEM. P26 *Tor1a*$^{+/+}$ mice N = 3, 25 ms: 1.24 ± 0.20, n = 5; 50 ms: 1.20 ± 0.12, n = 5, Student's t test p<0.05; P26 *Tor1a*$^{+/\Delta gag}$ mice N = 3, 25 ms: 1.22 ± 0.05, n = 5; 50 ms: 1.19 ± 0.08, n = 5; Student's t test p<0.05. Insets represent sample traces showing facilitation at ISI = 50 ms in both genotypes. (**C**) Representative sEPSCs recordings in PTX from SPNs of P26 *Tor1a*$^{+/+}$ and *Tor1a*$^{+/\Delta gag}$ mice. HP: −70 mV. The summary plots show no significant difference between genotypes in sEPSCs frequency and amplitude (Student's t test p>0.05). (**D**) Representative whole-cell recordings in PTX plus TTX of mEPSC from P26 *Tor1a*$^{+/+}$ and *Tor1a*$^{+/\Delta gag}$ SPNs. HP: −70 mV. Plots show a significant difference in the amplitude of mEPSCs recorded from *Tor1a*$^{+/\Delta gag}$ mice compared to wild-types (*Tor1a*$^{+/+}$, 7.45 ± 1.09, N = 9, n = 9; *Tor1a*$^{+/\Delta gag}$, 10.11 ± 0.97, N = 8, n = 9; Student's t test *p<0.05). (**E**) Representative recordings in MK-801 and CNQX of sIPSCs from P26 *Tor1a*$^{+/+}$ and *Tor1a*$^{+/\Delta gag}$ SPNs. HP:+10 mV. The summary plots show no significant difference in sIPSC frequency and amplitude (Student's t test p>0.05). (**F**) Representative traces of mIPSCs recorded in MK-801, CNQX and TTX. HP:+10 mV. The summary plots show no difference in frequency and amplitude between genotypes (Student's t test p>0.05). Data are presented as mean ± SEM.

DOI: https://doi.org/10.7554/eLife.33331.002

The following source data is available for figure 1:

Source data 1. Electrophysiological and synaptic properties of striatal SPNs.

DOI: https://doi.org/10.7554/eLife.33331.003

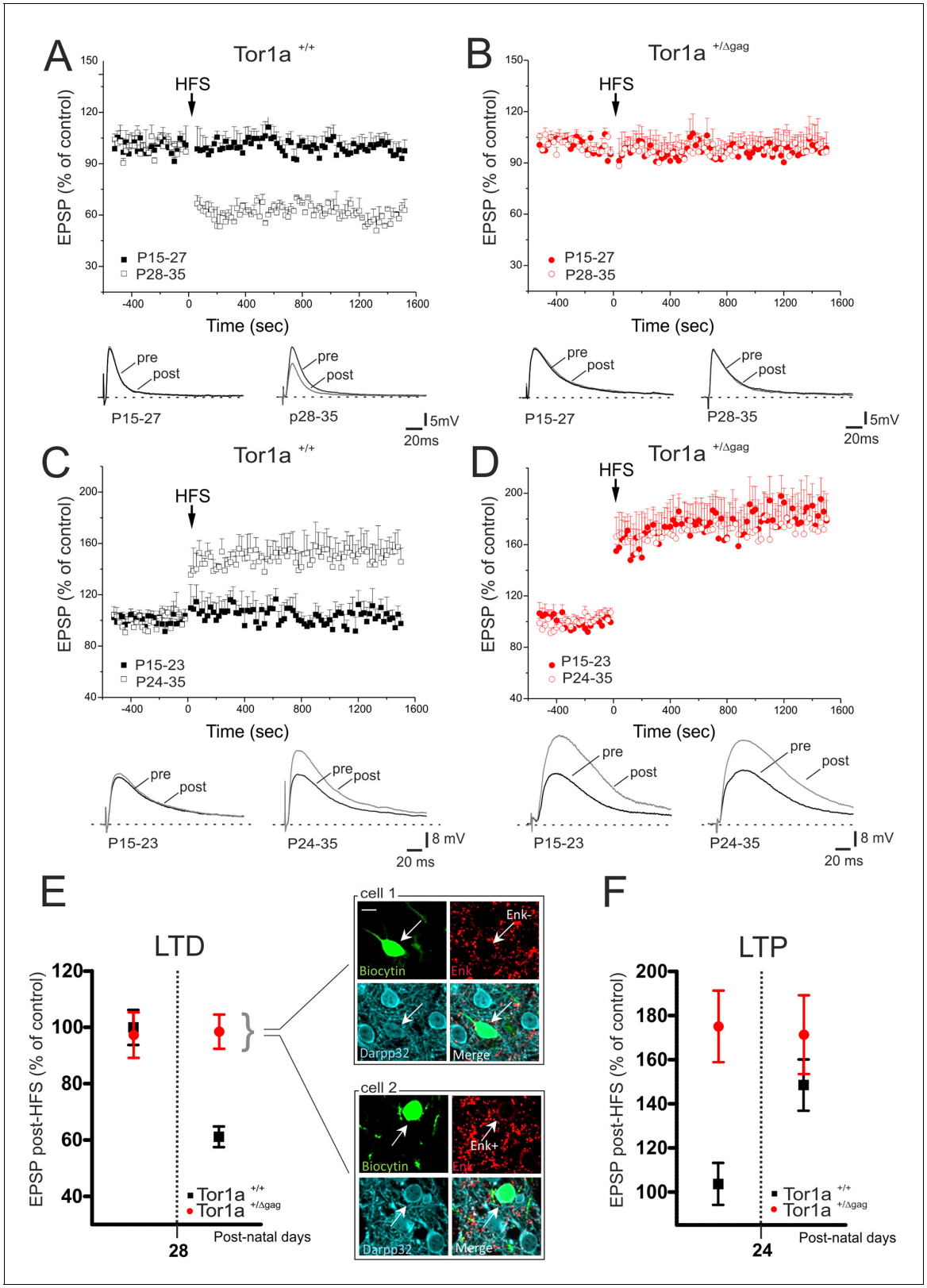

Figure 2. Altered developmental profile of corticostriatal long-term synaptic plasticity expression in *Tor1a*$^{+/\Delta gag}$ mice. (**A**) (*Top*) Developmental time-course of LTD expression in *Tor1a*$^{+/+}$ mice. HFS protocol (arrow) induces LTD in SPNs recorded from *Tor1a*$^{+/+}$ mice after P28 (59.63 ± 2.63% of control; N = 8, n = 8; paired Student's t test $p<0.05$), but not from P15 to P27 (99.46 ± 4.65, N = 9, n = 10; paired Student's t test $p>0.05$). (*Bottom*) Representative EPSP traces recorded before (pre) and 20 min after (post) HFS protocol delivery. (**B**) (*Top*) In *Tor1a*$^{+/\Delta gag}$ mice, HFS protocol fails to

Figure 2 continued on next page

Figure 2 continued

induce any LTD, irrespective of the postnatal age (P15-27, 96.85 ± 11.35% of control; N = 8, n = 12; P28-35, 100.29 ± 4.16% of control, N = 8, n = 12; paired Student's t test p>0.05). (*Bottom*) Representative traces of EPSPs recorded pre- and post-HFS. (**C**) (*Top*) Time-course of corticostriatal LTP expression during postnatal development in *Tor1a*$^{+/+}$ mice. HFS of corticostriatal afferents (*arrow*) induces LTP expression in *Tor1a*$^{+/+}$ mice after P24 (148.80 ± 15.39% of control; N = 6, n = 10; paired Student's t test p<0.05), but not at P15-23 (104.68 ± 8.99% of control; N = 6, n = 10; paired Student's t test p>0.05). (*Bottom*) Sample EPSPs recorded pre- and post-HFS protocol in *Tor1a*$^{+/+}$ mice. (**D**) (*Top*) SPNs recorded from *Tor1a*$^{+/\Delta gag}$ mice exhibit a premature LTP (P15-23, 174.68 ± 22.59% of control; N = 6, n = 10; P24-35, 172.35 ± 11.06% of control; N = 9, n = 10; paired Student's t test p<0.05). (*Bottom*) EPSP traces recorded pre- and post-LTP induction. (**E**) Mean plot comparing LTD expression at different postnatal days in *Tor1a*$^{+/+}$ and *Tor1a*$^{+/\Delta gag}$ SPNs. (*Inset*) Confocal imaging of two SPNs recorded from *Tor1a*$^{+/\Delta gag}$ slices filled with biocytin (green) and immunolabelled for ENK (red) and DARPP-32 (cyano), marker of SPNs. Both ENK-positive and ENK-negative biocytin-labeled SPNs showed lack of LTD (scale bar: 10 μm). (**F**) Mean plot comparing LTP expression at different postnatal days in *Tor1a*$^{+/+}$ and *Tor1a*$^{+/\Delta gag}$ SPNs. Values are presented as mean ± SEM.

DOI: https://doi.org/10.7554/eLife.33331.004

The following source data is available for figure 2:

Source data 1. Altered developmental profile of corticostriatal long-term synaptic plasticity expression in *Tor1a*$^{+/\Delta gag}$ mice.

DOI: https://doi.org/10.7554/eLife.33331.005

The LTP induction protocol failed to elicit a potentiation in *Tor1a*$^{+/+}$ mice from P15 to P23 (***Partridge et al., 2000***) (***Figure 2C***; p>0.05), whereas a stable LTP occurred from P24 to P35 (***Figure 2C***; 148.80 ± 15.39% of control; p<0.05). Unexpectedly, in *Tor1a*$^{+/\Delta gag}$ SPNs LTP could be evoked as early as P15, revealing a premature onset, and showed a tendency to increase, compared to wild types (***Figure 2D***; *Tor1a*$^{+/\Delta gag}$ P15-23, 174.68 ± 22.59% of control; P24-35, 172.35 ± 11.06% of control; p<0.05).

The pattern of torsinA expression is common to all striatal DARPP-32-labeled neurons (***Martella et al., 2009***). To unmask potential differences between direct- and indirect-pathway SPNs, recording electrodes were filled with biocytin. Enkephalin staining revealed that neither ENK-positive nor ENK-negative SPNs exhibited LTD, ruling out a possible segregation to a specific population of SPNs (***Figure 2E***).

Collectively, these data demonstrate that LTD appeared at P28 in wild-type mice, whereas it could not be elicited during the entire postnatal period of observation in *Tor1a*$^{+/\Delta gag}$ mice (***Figure 2E***). Moreover, while in *Tor1a*$^{+/+}$ mice LTP could not be evoked before P24, in SPNs from *Tor1a*$^{+/\Delta gag}$ LTP appeared prematurely at P15 (***Figure 2F***).

Increased AMPA receptor function and abundance at corticostriatal synapses during development

Changes in synaptic strength during learning and memory processes implicate an accurate regulation of AMPARs and NMDARs expression at postsynaptic membranes (***Bassani et al., 2013***; ***Czöndör and Thoumine, 2013***). Thus, we performed an electrophysiological and biochemical characterization of AMPARs and NMDARs of SPNs in both *Tor1a*$^{+/+}$ and *Tor1a*$^{+/\Delta gag}$ mice.

To investigate the relative abundance of postsynaptic AMPARs and NMDARs, NMDAR/AMPAR current ratios at corticostriatal synapses were evaluated in both juvenile (P26) and adult (P60) *Tor1a*$^{+/+}$ and *Tor1a*$^{+/\Delta gag}$ SPNs (***Figure 3A–B***). We found that, at P26, the NMDAR/AMPAR ratio was significantly reduced in *Tor1a*$^{+/\Delta gag}$ SPNs compared to wild types (***Figure 3A***; p<0.05). Conversely, no significant differences were recorded in P60 SPNs of both genotypes (***Figure 3B***; p>0.05). A reduced NMDAR/AMPAR ratio could reflect an increase in AMPAR function or number, a decrease in NMDARs function, or even a combination of both. To detect possible differences in the composition of postsynaptic glutamate receptors in P26 SPNs, a IV relationship of AMPAR-EPSC was recorded (***Figure 3C***). *Tor1a*$^{+/\Delta gag}$ SPNs showed a significantly increased current at hyperpolarized voltage ranges (***Figure 3C***; 2-way ANOVA, p<0.01;HP= −70 mV). The GluA2 subunit reduces AMPAR permeability to Ca^{2+}. Therefore, depending on the subunit composition, AMPAR-EPSC may show a linear or an inward-rectifying IV relationship (***Cull-Candy et al., 2006***). Thus, we measured the rectification index (RI), calculated as the ratio between the AMPAR-EPSC at −70 mV and at +40 mV (***Isaac et al., 2007***). We observed no significant difference in RI between genotypes (***Figure 3C***; p>0.05), suggesting that the enhanced AMPAR current involves an increased surface expression of AMPARs, rather than an altered receptor composition. Moreover, the AMPAR-EPSC IV relationship was also recorded in the presence of the selective antagonist of GluA2-lacking AMPARs, NASPM

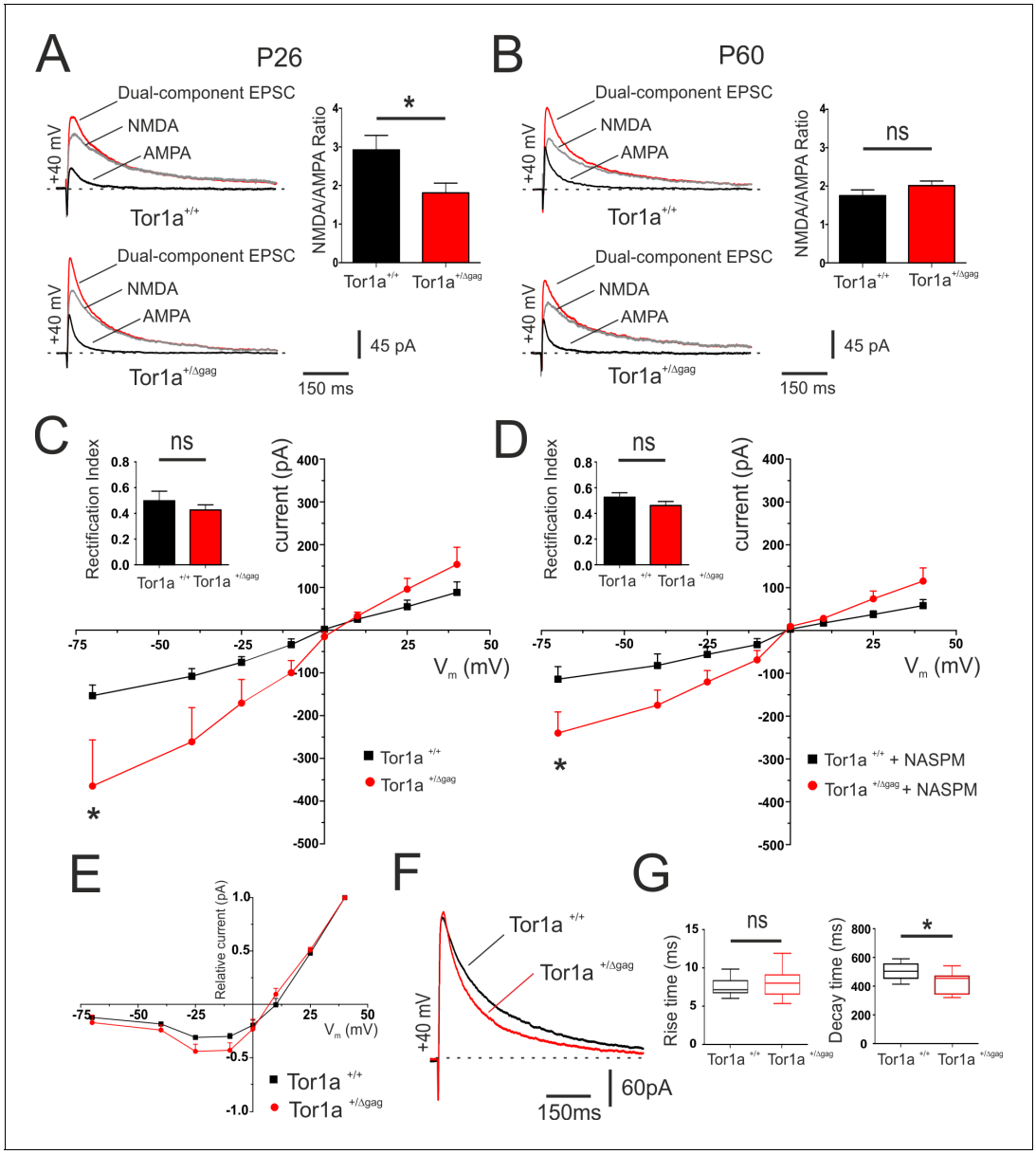

Figure 3. Electrophysiological characterization of AMPAR and NMDAR currents at corticostriatal synapses of SPNs in both *Tor1a*$^{+/+}$ and *Tor1a*$^{+/\Delta gag}$ mice. (**A**) (*Left*) Representative EPSCs traces recorded at HP=+40 mV from SPNs of juvenile *Tor1a*$^{+/+}$ and *Tor1a*$^{+/\Delta gag}$ mice. The NMDAR antagonist MK-801 isolates the AMPAR-mediated EPSC component (black trace), while the NMDAR-EPSC (grey trace) is obtained by digital subtraction of the AMPAR EPSC from the dual-component EPSC (red). (*Right*) Summary plot of NMDA/AMPA current ratio calculated in SPNs from P26 *Tor1a*$^{+/+}$ and *Tor1a*$^{+/\Delta gag}$ mice. A significant decrease of NMDA/AMPA ratio was detected in P26 *Tor1a*$^{+/\Delta gag}$ mice, compared to *Tor1a*$^{+/+}$ (*Tor1a*$^{+/+}$, 2.92 ± 0.38, N = 3, n = 8; *Tor1a*$^{+/\Delta gag}$, 1.81 ± 0.25, N = 3, n = 6; Student's t test, p<0.05). (**B**) (*Left*) Representative EPSCs traces recorded at HP =+40 mV from SPNs of adult *Tor1a*$^{+/+}$ and *Tor1a*$^{+/\Delta gag}$ mice. (*Right*) Summary plot of NMDA/AMPA current ratio showing no significant difference between genotypes (*Tor1a*$^{+/+}$, 1.75 ± 0.15, N = 3, n = 7; *Tor1a*$^{+/\Delta gag}$, 2.01 ± 0.12, N = 3, n = 7; Student's t test, p>0.05). (**C**) AMPAR-mediated currents recorded at different HP in P26 *Tor1a*$^{+/+}$ and *Tor1a*$^{+/\Delta gag}$ SPNs. The IV relationship shows a significant increase in the current recorded at more hyperpolarized range from P26 *Tor1a*$^{+/\Delta gag}$ SPNs (HP=−70 mV: two-way ANOVA, *p<0.01). (*Left*) Summary plot of rectification index values of P26 *Tor1a*$^{+/+}$ and *Tor1a*$^{+/\Delta gag}$ SPNs (*Tor1a*$^{+/+}$, 0.50 ± 0.07, n = 7; *Tor1a*$^{+/\Delta gag}$, 0.43 ± 0.04, n = 8; Student's t test p>0.05). (**D**) AMPAR-mediated currents recorded in the presence of the GluA2-lacking AMPAR antagonist NASPM at P26. HP =−70 mV; to-way ANOVA, *p<0.01). (*Left*) Summary plots of the rectification index measured at P26 (*Tor1a*$^{+/+}$, 0.53 ± 0.04, n = 5, N = 6; *Tor1a*$^{+/\Delta gag}$, 0.46 ± 0.03, n = 7; Student's t test, p>0.05). (**E**) Normalized IV relationships of NMDAR-mediated currents show no difference between genotypes at P26 (two-way ANOVA, p>0.05). (**F**) Representative NMDA-mediated EPSCs recorded at HP =+40 mV from P26 SPNs. (**G**) Summary plots display rise and decay time of NMDA-EPSCs recorded at HP =+40 mV in SPNs from P26 *Tor1a*$^{+/+}$ and *Tor1a*$^{+/\Delta gag}$ mice (rise time: *Tor1a*$^{+/+}$, 7.78 ± 0.42, n = 9; *Tor1a*$^{+/\Delta gag}$, 9.23 ± 1.37, n = 7; Student's t test p>0.05; decay time: *Tor1a*$^{+/+}$, 502.50 ± 20.06, n = 9; *Tor1a*$^{+/\Delta gag}$, 422.10 ± 30.15, n = 7, Student's t test, *p<0.05). Values are presented as mean ± SEM.

Figure 3 continued on next page

Figure 3 continued

DOI: https://doi.org/10.7554/eLife.33331.006

The following source data is available for figure 3:

Source data 1. Electrophysiological characterization of AMPAR and NMDAR currents at corticostriatal synapses of SPNs in both *Tor1a*$^{+/+}$ and *Tor1a*$^{+/\Delta gag}$ mice.

DOI: https://doi.org/10.7554/eLife.33331.007

(100 µM). No significant difference in the RI of P26 SPNs was measured in the presence of NASPM (***Figure 3D***; p>0.05); yet, at hyperpolarized voltage ranges AMPAR-mediated current was still increased in *Tor1a*$^{+/\Delta gag}$ SPNs (***Figure 3D***; two-way ANOVA, p<0.01 at HP =−70 mV). These results further excluded possible alterations of AMPAR surface composition.

The normalized IV relationship of NMDAR-EPSCs showed the characteristic 'J-shape' (***Mayer et al., 1984***) in SPNs recorded at P26 from both genotypes (***Figure 3E***). No significant difference was found in the voltage-dependence of NMDARs (p>0.05). By analyzing the kinetics of the response at HP =+ 40 mV, we detected a significantly decreased decay time in *Tor1a*$^{+/\Delta gag}$ mice compared to controls (***Figure 3F,G***; p<0.05), despite a comparable rise time, suggesting a modification of NMDAR subunit composition (***Paoletti et al., 2013***). In particular, it is well-established that the decay time of NMDAR currents is correlated to the amount of GluN2-type subunits. GluN2A and GluN2B represent the most abundant NMDAR regulatory subunits expressed in SPNs (***Chen and Reiner, 1996***; ***Dunah and Standaert, 2003***) and are characterized by a fast and slow decay time, respectively (***Sanz-Clemente et al., 2013***).

Taking into account all the above-described electrophysiological results, we evaluated the levels of AMPAR and NMDAR subunits into TIF fractions purified from striata of both juvenile (P26) and adult (P60) mice by means of WB analysis. We found a significant increase in the levels of both GluA1 and GluA2 AMPAR subunits in the postsynaptic compartment of P26 *Tor1a*$^{+/\Delta gag}$ mice compared to controls (***Figure 4A,B***; p<0.05), consistent with the observed reduction of the NMDA/AMPA ratio and the absence of any alteration of the RI (see ***Figure 3***). Interestingly, we also found an increase of phosphorylation at GluA1-Ser845 (***Figure 4A,B***;, p<0.05), which is known to be correlated with LTP expression and to prevent endocytosis of GluA1-containing AMPARs (***Oh et al., 2006***; ***Bassani et al., 2013***). Moreover, in agreement with the reduction of the NMDAR decay time, we observed an increase of GluN2A but not GluN2B subunit at postsynaptic sites of P26 *Tor1a*$^{+/\Delta gag}$ mice compared to *Tor1a*$^{+/+}$ (***Figure 4C,D***; p<0.05). Finally, no modifications of PSD-95, the most abundant scaffolding protein at the excitatory synapse, was observed (***Figure 4C,D***). Notably, these alterations of AMPAR and NMDAR subunits were not present in SPNs from P60 *Tor1a*$^{+/\Delta gag}$ mice (***Figure 4***; p>0.05).

Next, we performed a detailed evaluation of dendritic spine density and morphology in *Tor1a*$^{+/\Delta gag}$ SPNs, compared to age-matched *Tor1a*$^{+/+}$ mice. P26 *Tor1a*$^{+/\Delta gag}$ SPNs (***Figure 5A–D***) exhibited a higher number of mushroom-type spines (***Figure 5C***; p<0.05) and, consequently, a concomitant overall increase of dendritic spine width compared to *Tor1a*$^{+/+}$ mice (***Figure 5B***; p<0.05), thus suggesting an advanced stage of spine maturation, in agreement with the observed molecular GluN2A/GluN2B switch (see ***Figure 4***). This event was associated, as expected, to an overall decrease of dendritic spine density (***Figure 5A***; p<0.05).

Conversely, P60 *Tor1a*$^{+/\Delta gag}$ mice (***Figure 5E–H***) showed a normalization of dendritic spine density (***Figure 5E***; p>0.05) and of spine width (***Figure 5F***; p>0.05) compared to *Tor1a*$^{+/+}$ mice. Furthermore, with respect to P26, at P60 the number of mushrooms remained unchanged in *Tor1a*$^{+/\Delta gag}$ mice but increased in *Tor1a*$^{+/+}$ (***Figure 5G***; p<0.05). Yet, at P60 *Tor1a*$^{+/\Delta gag}$ mice showed an increase of thin spines compared to *Tor1a*$^{+/+}$ mice (***Figure 5G***; p<0.05).

Increased BDNF protein expression in Tor1a$^{+/\Delta gag}$ striatum at P26

Neurotrophic factors play a fundamental role in the development of SPNs and synaptic plasticity maturation (***Altar et al., 1997***; ***Rauskolb et al., 2010***). Particularly, BDNF contributes to the developmental expression of AMPAR subunits at postsynaptic compartments (***Jourdi et al., 2003***; ***Jourdi and Kabbaj, 2013***). The majority of BDNF, anterogradely transported to the striatum, originates from the cortex, where its expression begins in the first postnatal days (***Baydyuk and Xu,***

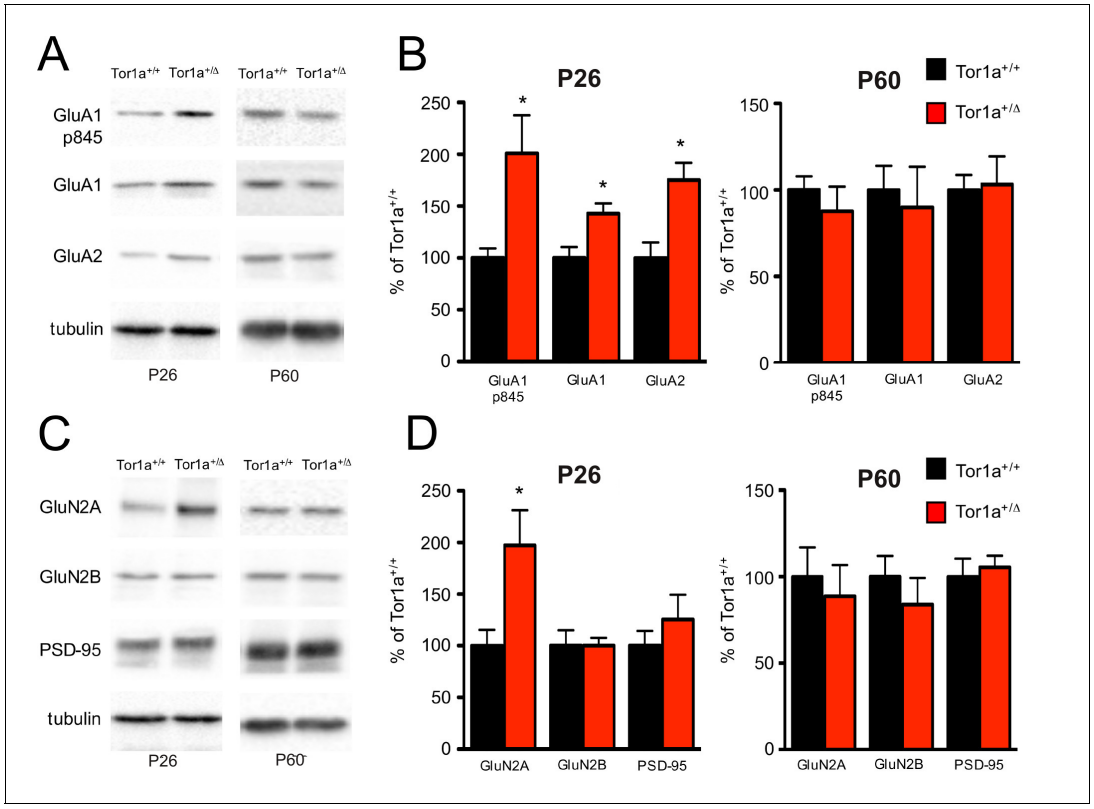

Figure 4. Molecular analysis of the SPNs postsynaptic compartment in P26 and P60 *Tor1a*$^{+/\Delta gag}$ compared to age-matched wild-type mice. WB analyses were performed on the post-synaptic TIF fraction in a minimum of three different animals per genotype. (**A**) WB analysis for GluN2A, GluN2B, PSD-95 and tubulin in P26 (left panel) and P60 (right panel) *Tor1a*$^{+/\Delta gag}$ and age-matched *Tor1a*$^{+/+}$ mice. (**C**) WB analysis for GluA1, GluA1p845, GluA2 and tubulin in P26 (left panel) and P60 (right panel) *Tor1a*$^{+/\Delta gag}$ and age-matched *Tor1a*$^{+/+}$ mice. (**B,D**) The histogram shows the quantification of protein levels following normalization on tubulin (P26 *Tor1a*$^{+/\Delta gag}$ compared to *Tor1a*$^{+/+}$, GluA1: 142.8 ± 9.8%, n = 5, p<0.05; GluA1-p845: 200.9 ± 36.6%, n = 5, p<0.05; GluA2: 175.1 ± 16.6%, n = 5, p<0.05; GluN2A: 197.3 ± 34.0%, n = 5, p<0.05; P60 *Tor1a*$^{+/\Delta gag}$ GluA1: 90.0 ± 23.4%, n = 5, p>0.05; GluA1-p845: 77.7 ± 14.2%, n = 5, p>0.05; GluA2: 103.2 ± 16.2%, n = 5, p>0.05; GluN2A: 88.8 ± 18.0%, n = 5,p>0.05). All values are mean ± SEM expressed as % of *Tor1a*$^{+/+}$ mice.

DOI: https://doi.org/10.7554/eLife.33331.008

2014). We first performed a WB time-course analysis of BDNF protein level in P15, P26 and adult (P60-P75) striatum. BDNF expression profile showed a similar age-dependent time-course in both genotypes (***Figure 6A,B***; P15 *vs* P26: *Tor1a*$^{+/+}$ p<0.05; *Tor1a*$^{+/\Delta gag}$p<0.01). As indicated by the BDNF/proBDNF ratio, in line with previous evidence (***Zermeño et al., 2009***), BDNF was highly expressed at P15 in both strains. At P26 the signal decreased, and then reached intermediate values in adults (***Figure 6A,B***).

Next, we compared striatal proBDNF and BDNF protein levels between genotypes at P26. In line with previous evidence, proBDNF was detected as a double band at ~32 KDa, whereas mature BDNF as a single band at 14 KDa (***Hartog et al., 2009***; ***Koshimizu et al., 2009***; ***Mandel et al., 2009***; ***Tropea et al., 2011***) (***Figure 6C***). Both proBDNF and BDNF levels were increased at P26 in *Tor1a*$^{+/\Delta gag}$ striatum (***Figure 6C***; proBDNF p<0.01, BDNF p<0.05). We therefore examined Bdnf mRNA expression in *Tor1a*$^{+/\Delta gag}$ cortex. Quantitative PCR revealed an increased Bdnf expression in *Tor1a*$^{+/\Delta gag}$ cortex as compared to *Tor1a*$^{+/+}$ (***Figure 6D***; p<0.05). No significant difference between genotypes was measured in the proBDNF and BDNF striatal protein levels in adult mice (***Figure 6E***; p>0.05). Collectively, these data indicate an increase of BDNF level in P26 *Tor1a*$^{+/\Delta gag}$ striatum.

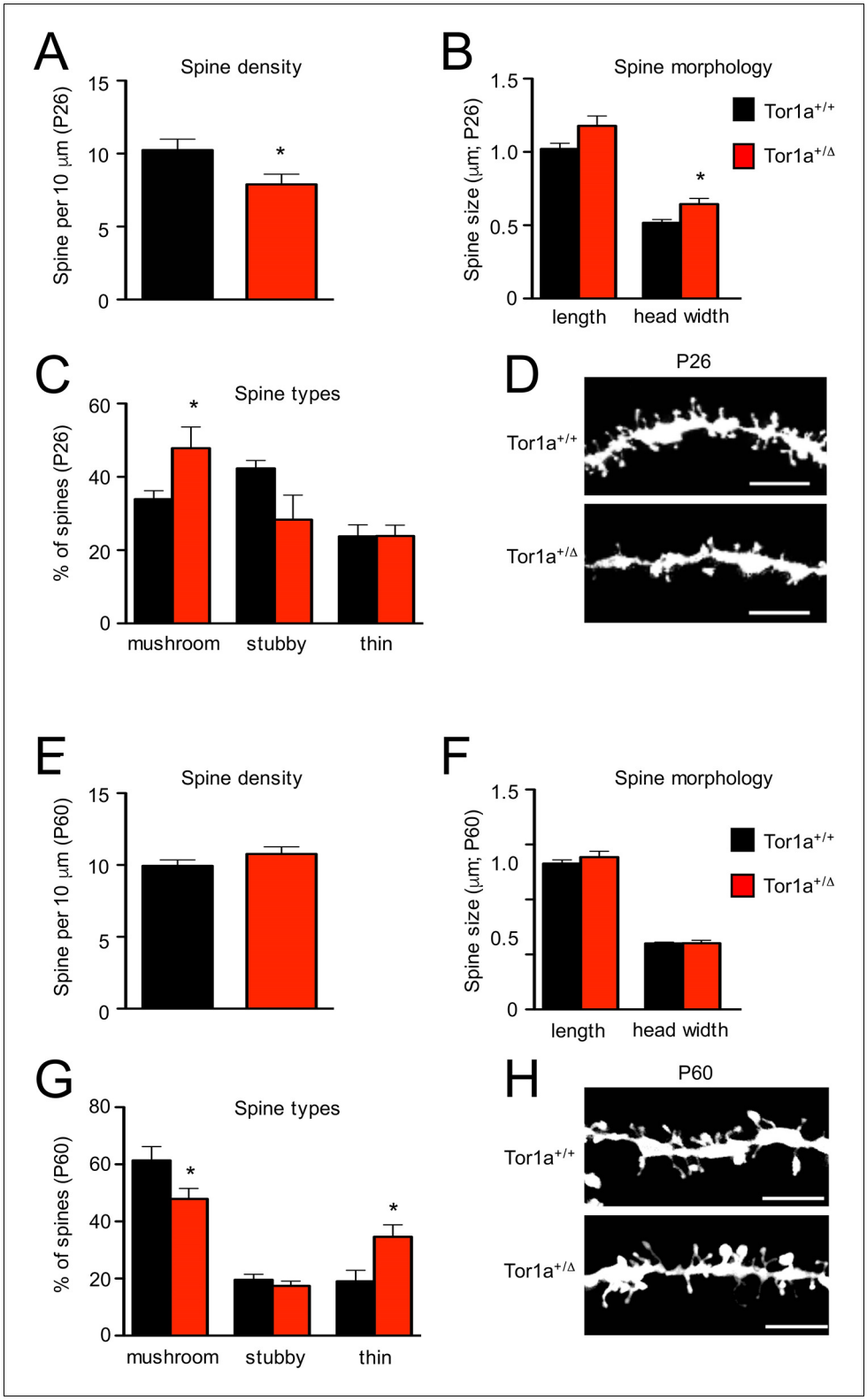

Figure 5. Analysis of dendritic spines morphology in P26 and P60 *Tor1a*$^{+/\Delta gag}$ compared to age-matched *Tor1a*$^{+/+}$mice. (**A**) Histogram representing dendritic spine density in P26 *Tor1a*$^{+/\Delta gag}$ and *Tor1a*$^{+/+}$ mice (*Tor1a*$^{+/+}$, 10.25 ± 0.75 spines/10 µm, n = 10; *Tor1a*$^{+/\Delta gag}$, 7.89 ± 0.70 spines/10 µm, n = 10; unpaired Student's t test *p<0.05). (**B,C**) Histograms showing the quantification of dendritic spine size (B, spine length and head width) and dendritic spine type (C, mushroom, stubby, thin) in P26 *Tor1a*$^{+/\Delta gag}$ compared to *Tor1a*$^{+/+}$ mice (dendritic spine

Figure 5 continued on next page

Figure 5 continued

width *Tor1a*$^{+/+}$, 0.51 ± 0.02 µm, n = 10; *Tor1a*$^{+/\Delta gag}$, 0.64 ± 0.04 µm, n = 10, unpaired Student's t-test *p<0.05; mushroom-type spines *Tor1a*$^{+/+}$, 33.92 ± 2.32%, n = 10; *Tor1a*$^{+/\Delta gag}$, 47.81 ± 5.79%, n = 10, unpaired Student's t-test *p<0.05). (**D**) Representative images show dendrites of P26 *Tor1a*$^{+/\Delta gag}$ and *Tor1a*$^{+/+}$ mice. (**E**) Histogram representing dendritic spine density in P60 *Tor1a*$^{+/\Delta gag}$ and *Tor1a*$^{+/+}$ mice (*Tor1a*$^{+/+}$, 9.94 ± 0.41 spines/10 µm, n = 10; *Tor1a*$^{+/\Delta gag}$, 10.76 ± 0.50 spines/10 µm, n = 10; unpaired Student's t-test p>0.05). (**F,G**) Histograms showing the quantification of dendritic spine size (F, spine length and head width) and dendritic spine type (G, mushroom, stubby, thin) in P60 *Tor1a*$^{+/\Delta gag}$, compared to *Tor1a*$^{+/+}$ mice (spine width *Tor1a*$^{+/+}$, 0.600 ± 0.012 µm, n = 10; *Tor1a*$^{+/\Delta gag}$, 0.602 ± 0.027 µm, n = 10; p>0.05; mushroom-type spines *Tor1a*$^{+/+}$, 61.40 ± 4.81%, n = 10; *Tor1a*$^{+/\Delta gag}$, 47.92 ± 3.67%, n = 10; *p<0.05; thin spines *Tor1a*$^{+/+}$, 19.04 ± 3.85%, n = 10; *Tor1a*$^{+/\Delta gag}$, 34.64 ± 4.16%, n = 10; *p<0.05; unpaired Student's t-test). (**H**) Representative images show dendrites of P60 *Tor1a*$^{+/\Delta gag}$ and *Tor1a*$^{+/+}$ mice. Data were collected in a minimum of three different animals per genotype.

DOI: https://doi.org/10.7554/eLife.33331.009

The following source data is available for figure 5:

Source data 1. Analysis of dendritic spines morphology in P26 *Tor1a*$^{+/\Delta gag}$ compared to age-matched *Tor1a*$^{+/+}$ mice.

DOI: https://doi.org/10.7554/eLife.33331.010

Source data 2. Analysis of dendritic spines morphology in P60 *Tor1a*$^{+/\Delta gag}$ compared to age-matched *Tor1a*$^{+/+}$ mice.

DOI: https://doi.org/10.7554/eLife.33331.011

BDNF regulates surface AMPA receptor expression and synaptic plasticity

BDNF has been shown to contribute to LTP induction in normal mice (***Jia et al., 2010***). To test whether the increase in BDNF levels was involved in the abnormal regulation of AMPA currents and in the synaptic plasticity deficits, BDNF signalling was selectively blocked by the tropomyosin-related kinase B (TrkB) receptor competitive antagonist, ANA-12 (***Cazorla et al., 2011***). A single in vivo administration of ANA-12 (0.5 mg/kg, intraperitoneal, 4 hr before the experiment) failed to rescue synaptic plasticity deficits in young *Tor1a*$^{+/\Delta gag}$ mice (data not shown). However, repetitive treatment with ANA-12 (0.5 mg/kg, intraperitoneal, 12 hr and 4 hr before the experiment; ***Cazorla et al., 2011***; ***Stragier et al., 2015***), completely rescued corticostriatal LTD expression in P28-35 *Tor1a*$^{+/\Delta gag}$ mice (***Figure 7A***; p<0.05). Additionally, ANA-12 treatment reduced LTP amplitude in P24-35 *Tor1a*$^{+/\Delta gag}$ mice (***Figure 7B***; p>0.05). In vehicle-treated *Tor1a*$^{+/+}$ and *Tor1a*$^{+/\Delta gag}$ mice, no significant change was observed (data not shown).

Likewise, in vivo treatment with ANA-12 totally normalized the IV curve of AMPAR-EPSC in P26 *Tor1a*$^{+/\Delta gag}$ mice (***Figure 7C***; p>0.05). Accordingly, also the RI displayed no significant difference between genotypes (***Figure 7C***; p>0.05). These findings suggest that increased BDNF levels are involved in the abnormal developmental expression of AMPARs on SPN postsynaptic membranes, leading to synaptic plasticity alterations in juvenile mice.

Finally, to demonstrate that BDNF alterations occur in a defined time-window, we tested the effect of ANA-12 on corticostriatal LTD expression in adult *Tor1a*$^{+/\Delta gag}$ mice. In vivo treatment with ANA-12 (0.5 mg/kg, intraperitoneal, two administrations at 12 hr and 4 hr before the experiment) failed to restore corticostriatal LTD in P60 *Tor1a*$^{+/\Delta gag}$ mice (***Figure 7D***; p>0.05) confirming that BDNF-dependent alterations are limited to a sensitive period.

Cholinergic transmission is not involved in the early phase of synaptic plasticity alterations

Previous work demonstrated a prominent involvement of cholinergic transmission in the impairment of striatal synaptic plasticity in adult *Tor1a*$^{+/\Delta gag}$ mice (***Maltese et al., 2014***). To verify whether plasticity alterations in juvenile *Tor1a*$^{+/\Delta gag}$ mice could also involve cholinergic signaling, slices were pretreated with the M1 muscarinic receptor antagonist, pirenzepine (100 nM, 20 min). Pirenzepine failed to rescue the expression of LTD in *Tor1a*$^{+/\Delta gag}$ mice from p28 to p35 (***Figure 7E***; p>0.05), indicating that distinct mechanisms underlie plasticity alterations at different developmental stages.

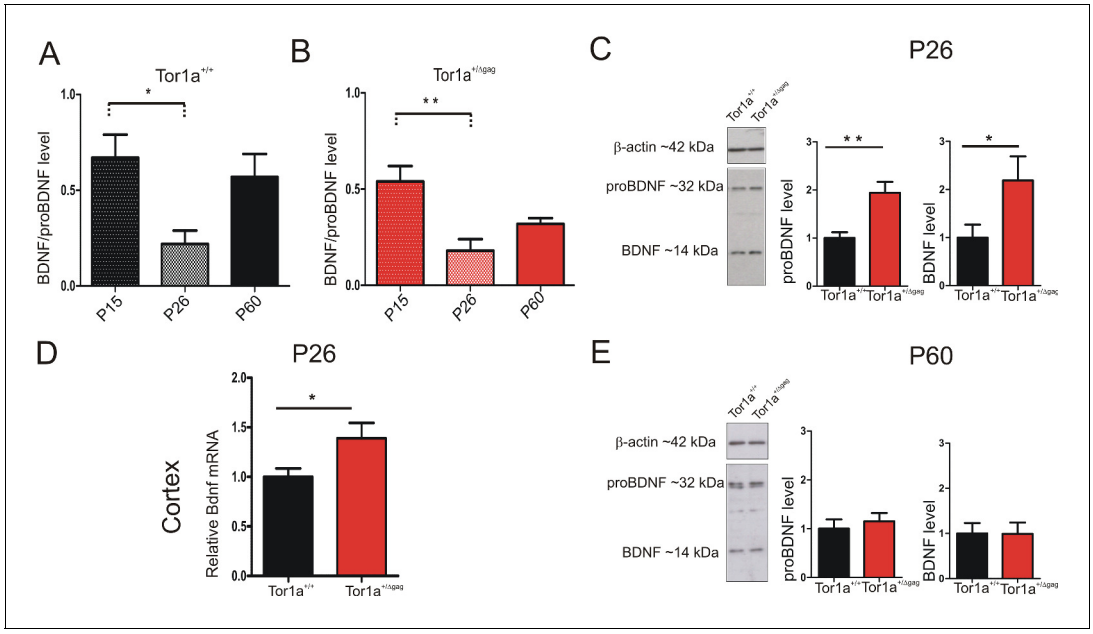

Figure 6. BDNF protein expression in the striatum of *Tor1a*$^{+/+}$and *Tor1a*$^{+/\Delta gag}$ mice. (**A, B**) Striatal BDNF protein expression in *Tor1a*$^{+/+}$ and *Tor1a*$^{+/\Delta gag}$ mice at postnatal stages (**P15, P26, P60**). The graphs show the quantification of BDNF/proBDNF ratio at the various ages. Data are represented as mean ± SEM (*Tor1a*$^{+/+}$ P15: 0.67 ± 0.12, N = 4; P26: 0.22 ± 0.08, N = 4; P60: 0.57 ± 0.14, N = 3; *Tor1a*$^{+/\Delta gag}$ P15: 0.54 ± 0.08, N = 4; P26: 0.18 ± 0.06, N = 4; P60: 0.32 ± 0.03, N = 4; one-way ANOVA, *p<0.05; **p<0.01). (**C**) (*Left*) Representative WB of proBDNF and BDNF protein levels relative to β-actin in striatal extracts (30 µg) derived from P26 *Tor1a*$^{+/+}$ and *Tor1a*$^{+/\Delta gag}$ mice. (*Right*) The graphs show the quantitative analysis. The amount of proBDNF and BDNF was quantified relative to β-actin and normalized to wild-type mice. Data are represented as mean ± SEM (proBDNF *Tor1a*$^{+/+}$ 1.00 ± 0.12, n = 10; Tor1a$^{+/\Delta gag}$1.95 ± 0.29, n = 8; BDNF Tor1a$^{+/+}$: 1.00 ± 0.28, n = 8, *Tor1a*$^{+/\Delta gag}$2.19 ± 0.50, n = 8, Student's t test: *p<0.05; **p<0.01). (**D**) Bdnf mRNA is upregulated in the cortex of *Tor1a*$^{+/\Delta gag}$ determined by qRT-PCR. The $2^{-\Delta\Delta Ct}$ method was used to determine the relative expression, and all of the values are expressed relative to the levels of the wild-type mice as mean ± SEM (*Tor1a*$^{+/+}$ 1.000 ± 0.084, n = 10; *Tor1a*$^{+/\Delta gag}$1.399 ± 0.163, n = 8; Student's t test: *p<0.05). (**E**) (*Left*) Representative Western blots of proBDNF and BDNF proteins relative to β-actin in striatal extracts (15 µg) derived from *Tor1a*$^{+/+}$ and *Tor1a*$^{+/\Delta gag}$ adult mice. (*Right*) The graphs show the quantitative analysis. The amount of proBDNF and BDNF was quantified relative to β-actin and normalized to wild-type mice. Data are represented as mean ± SEM (proBDNF *Tor1a*$^{+/+}$ 1.00 ± 0.19, n = 7, *Tor1a*$^{+/\Delta gag}$1.15 ± 0.17, n = 7, p>0.05; BDNF *Tor1a*$^{+/+}$: 1.00 ± 0.23 n = 7, *Tor1a*$^{+/\Delta gag}$0.99 ± 0.25, n = 7, Student's t test: p>0.05).

DOI: https://doi.org/10.7554/eLife.33331.012

The following source data is available for figure 6:

Source data 1. BDNF protein expression in the striatum of *Tor1a*$^{+/+}$ and *Tor1a*$^{+/\Delta gag}$ mice.

DOI: https://doi.org/10.7554/eLife.33331.013

Discussion

The critical period for the onset of symptoms in DYT1 dystonia patients matches an early time-window of activity-dependent plastic changes in the striatum, which shape motor memory and learning processes during childhood and early adolescence.

Our systematic analysis of functional and structural synaptic plasticity in DYT1 dystonia demonstrates: (i) The existence of a critical period when SPNs exhibit premature LTP; (ii) A significant increase of AMPAR levels in the postsynaptic compartment which correlates with the reduction of NMDA/AMPA ratio, the increased amplitudes of postsynaptic currents and the rightward shift in the AMPA I-V curve observed in juvenile *Tor1a*$^{+/\Delta gag}$ mice; (iii) A BDNF time-dependent increase in expression profile, which parallels the alterations described; (iv) abnormal plasticity is associated with profound changes of dendritic spine density and morphology in juvenile *Tor1a*$^{+/\Delta gag}$; (v) A rescue of the synaptic plasticity deficits is obtained by in vivo administration of a TrkB inhibitor.

It is currently unknown why penetrance is only 30% in DYT1 mutation carriers. One possibility is that at circuit level, motor system is already impaired early during development. The existence of a defined period in which neurons are particularly susceptible to experience-driven modifications is well-established, concurrently with structural modifications, and is currently believed to represent a

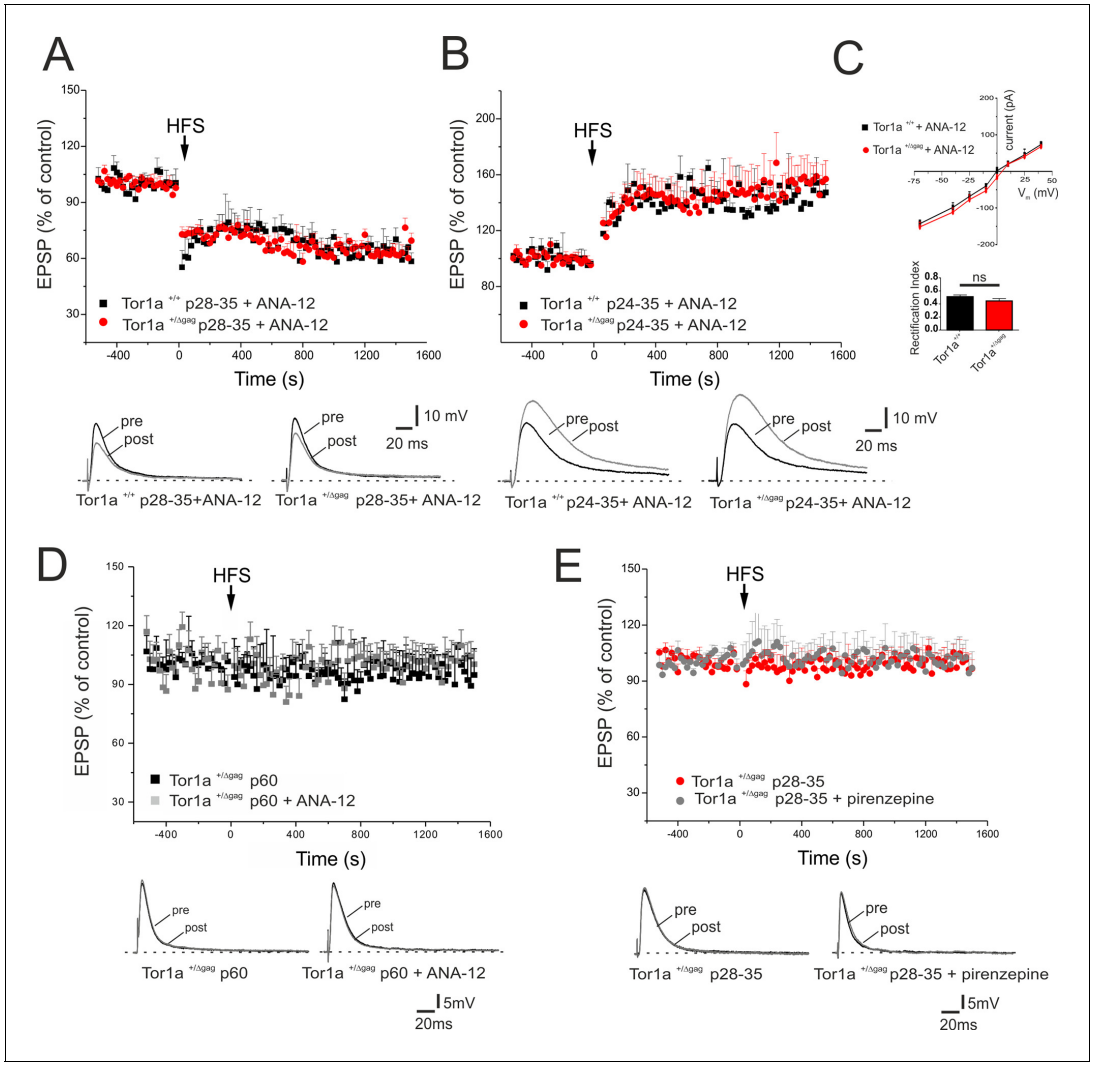

Figure 7. In vivo ANA-12 treatment rescues synaptic plasticity deficits in juvenile *Tor1a*$^{+/\Delta gag}$ mice. (**A**) Time-course of corticostriatal LTD in juvenile *Tor1a*$^{+/+}$ and *Tor1a*$^{+/\Delta gag}$ mice (P28-35): after in vivo treatment with the TrkB antagonist ANA-12, the HFS protocol (arrow) induces corticostriatal LTD expression in juvenile *Tor1a*$^{+/\Delta gag}$ mice (*Tor1a*$^{+/+}$ P28-35, 65.31 ± 1.44% of control; N = 3, n = 12, p<0.05; *Tor1a*$^{+/\Delta gag}$ P28-35, 63.41 ± 4.39% of control; N = 3, n = 10; paired Student's t test p<0.05). (*Bottom*) Representative EPSPs recorded before (pre) and 20 min after (post) HFS protocol. (**B**) Time-course of corticostriatal LTP after in vivo ANA-12 treatment: LTP displays a physiological amplitude in SPNs from in P24-35 *Tor1a*$^{+/\Delta gag}$ compared to wild-type littermates (*Tor1a*$^{+/+}$ P24-35, 144.55 ± 2.67% of control; N = 3, n = 8; *Tor1a*$^{+/\Delta gag}$ P24-35, 148.11 ± 10.55% of control; N = 3, n = 9; *Tor1a*$^{+/\Delta gag}$ *vs. Tor1a*$^{+/+}$ Student's t test p>0.05). (*Bottom*) Sample traces recorded pre and post LTP induction. (**C**) AMPAR-mediated currents recorded from P26 SPNs at HP from −70 mV to + 40 mV after in vivo treatment of *Tor1a*$^{+/+}$ and *Tor1a*$^{+/\Delta gag}$ mice with ANA-12. The treatment normalizes the current-voltage relationship in *Tor1a*$^{+/\Delta gag}$ neurons (HP=−70 mV: 2-way ANOVA p>0.05) and the rectification index (*Tor1a*$^{+/+}$, 0.51 ± 0.03, N = 3, n = 3; *Tor1a*$^{+/\Delta gag}$, 0.45 ± 0.04, N = 3, n = 5; Student's t test p>0.05) (**D**) In vivo treatment with ANA-12 does not restore corticostriatal LTD in adult (**P60**) SPNs recorded from *Tor1a*$^{+/\Delta gag}$ mice (vehicle: 95.66 ± 9.09% of control, N = 3, n = 8; ANA-12: 98.75 ± 11% of control, N = 3, n = 4; paired Student's t test p>0.05). (**E**) Slice pre-treatment with pirenzepine (100 nM) does not rescue LTD expression in P28-35 *Tor1a*$^{+/\Delta gag}$ SPNs (vehicle: 101.54 ± 1.07% of control, N = 3, n = 3; pirenzepine: 100.34 ± 8.96% of control; N = 3, n = 3; paired Student's t test p>0.05). (*Bottom*) Superimposed traces of EPSPs recorded pre and 20 min post HFS delivery.

DOI: https://doi.org/10.7554/eLife.33331.014

The following source data is available for figure 7:

Source data 1. In vivo ANA-12 treatment rescues synaptic plasticity deficits in juvenile *Tor1a*$^{+/\Delta gag}$ mice.

DOI: https://doi.org/10.7554/eLife.33331.015

nodal mechanism both in physiological and pathological conditions (**Turrigiano and Nelson, 2004**; **Johnston, 2004**; **Meredith, 2015**; **Calabresi et al., 2016**).

Our electrophysiological assessment of synaptic plasticity identifies a rather narrow time-window, between P15 and P26 when striatal SPNs exhibit a premature LTP, whereas LTD cannot be evoked. Although it has to be cautiously reminded that these alterations match those described in adult DYT1 striata (**Martella et al., 2014**), the time-course performed in the present study indicates their abnormal early appearance, in a developmental phase when normal striatal SPNs do not yet exhibit long-lasting synaptic changes. Of interest, the loss of LTD was observed in a similar time frame in a novel model with a rare missense variant in the *Tor1a* gene (**Bhagat et al., 2016**).

Moreover, we describe, along with electrophysiological deficits, molecular and structural changes at striatal synapses that appear to be limited to a specific time-window. Striatal LTP either in mature tissue preparation or in the developing striatum is dependent on the activation of NMDAR (**Calabresi et al., 1992b**; **Partridge et al., 2000**), whereas LTD depends on AMPAR (**Calabresi et al., 1992a**). Our electrophysiological and biochemical characterization demonstrates an increase in currents mediated by AMPAR, consistent with the increased amplitude of mEPSCs, and additionally, the NMDAR/AMPAR ratio was significantly reduced in SPNs from DYT1 mice. A major mechanism regulating synaptic strength involves the balance between synaptic insertion and removal of glutamate receptors into the postsynaptic membrane (**Gong and De Camilli, 2008**). Specifically, loss of homeostatic regulation of excitatory synapses in distinct neuronal subtypes involve postsynaptic changes in accumulation of AMPAR (**Lissin et al., 1998**; **O'Brien et al., 1998**). Accordingly, we observed a significant increase of both GluA1 and GluA2 subunits of AMPARs in the postsynaptic compartment of P26 *Tor1a*$^{+/\Delta gag}$ mice compared to controls, suggestive of an increased surface expression of AMPARs. Of interest, the significant increase of the phosphorylation of GluA1-Ser845, a well-established correlate of LTP (**Oh et al., 2006**; **Bassani et al., 2013**) is consistent with the abnormal LTP expression measured in DYT1 mice. Moreover, GluA1-Ser845 (**Roche et al., 1996**) plays a key role in the synaptic delivery of GluA1-containing AMPARs by LTP (**Esteban et al., 2003**; **Bassani et al., 2013**) and is involved in surface reinsertion/stabilization of AMPARs (**Ehlers, 2000**), thus providing a molecular mechanism for the observed increase of AMPARs at postsynaptic membranes in P26 *Tor1a*$^{+/\Delta gag}$ mice compared to controls. Thus, we hypothesize that the loss of LTD may be related to the aberrant composition of striatal AMPARs observed in mutant mice.

The identification of increased AMPAR subunit levels in the postsynaptic compartment offers new opportunities to identify potential regulators of AMPAR turnover. Neurotrophins have been implicated in glutamatergic synapse development and plasticity, suggesting a potential role in postsynaptic proteins distribution (**Causing et al., 1997**; **McAllister et al., 1997**; **Kong et al., 2001**). Previous work elucidated the role of BDNF in the regulation of AMPAR expression and function, including synaptic AMPAR subunit trafficking (**Narisawa-Saito et al., 1999**; **Jourdi and Kabbaj, 2013**). Indeed, BDNF treatment acutely controls both AMPAR subunits and their scaffolding proteins trafficking, thereby modifying the strength of synaptic activity (**Minichiello et al., 1999**; **Mauceri et al., 2004**). Remarkably, we observed an enhancement of pro-BDNF and BDNF protein level in P26 *Tor1a*$^{+/\Delta gag}$ mice, which appears critical for the onset of abnormal neurophysiological phenotype in DYT1 dystonia. Consistently, we obtained a functional rescue of synaptic plasticity and AMPA-mediated currents with the competitive antagonist of BDNF TrkB receptor ANA-12 (**Cazorla et al., 2011**).

Activity-dependent synaptic plasticity as well as composition and activity of NMDARs and AMPARs strictly govern modifications of dendritic spine morphology, leading to a long-lasting structural plasticity. Yet, BDNF also plays a major role in spine maturation in several brain regions, including the striatum (**Baquet et al., 2004**; **Rauskolb et al., 2010**). Thus, the abnormal increase in BDNF expression fits with the abnormalities in spine morphology we observed. In P26 *Tor1a*$^{+/\Delta gag}$ mice, we measured an increase in mushroom spines, suggestive of a 'premature' maturation process accompanied by an overall decrease in the density of dendritic spines. It is well-known that expression patterns of the GluN2 subunits of NMDARs at dendritic spines change during the first postnatal weeks. In particular, GluN2A expression increases from the second postnatal week to become widely expressed and abundant throughout the brain (**Bellone and Nicoll, 2007**; **Gray et al., 2011**). Yet, in agreement with the reduction of the NMDAR decay time, we found an increase of postsynaptic GluN2A in P26 *Tor1a*$^{+/\Delta gag}$ mice suggesting a 'premature' GluN2A/GluN2B switch, thus indicating the existence of a molecular and morphological early maturation of the excitatory synapse in this

DYT1 model. Moreover, the existence of a close coordination between spine size and AMPAR levels at synaptic membranes has been previously reported (**Kopec et al., 2007**; **Malinverno et al., 2010**) and spine volume has been positively correlated with the strength of AMPAR-mediated synaptic transmission. Accordingly, in *Tor1a*$^{+/\Delta gag}$ mice we found a significant increase of spine head width, an increase in mushroom spines and a concomitant increase of both GluA1 and GluA2 subunits of AMPARs.

Most of the molecular and structural alterations described in juvenile DYT1 mice were not confirmed at our analyses performed in adult (P60) mice. Indeed, inhibition of BDNF with ANA-12 did not offset the plasticity deficits in adult mice. Additionally, the anticholinergic agent pirenzepine failed to rescue the plasticity deficits in juvenile animals, contrarily to what reported in adults (**Dang et al., 2012**; **Martella et al., 2014**), indicating that distinct mechanisms sustain the abnormal patterns of synaptic activity at different developmental ages. Future work is required to address the precise mechanisms governing this switch.

Collectively, we demonstrate that the rise of BDNF, in a restricted time-window, drives AMPA receptor composition changes and, consequently, structural modifications in spine morphology, resulting in the loss of homeostatic regulation of synaptic plasticity early in postnatal life.

Our hypothesis is also consistent with the clinical observation that the beneficial effects of Deep Brain Stimulation (DBS) in dystonic patients is more effective in young patients, as compared to patients implanted later in life (**Isaias et al., 2008**). Additionally, compared to the prompt efficacy observed in Parkinson's disease patients, weeks are commonly required to obtain symptomatic relief following DBS, and improvements may continue to be manifest over time (**Vercueil et al., 2001**; **Krauss, 2002**; **Vidailhet and Pollak, 2005**). It is plausible that severity of abnormal plasticity is related to disease duration, thus justifying the longer time required to erase aberrant plasticity patterns.

In a therapeutic perspective, these sensitive periods might be considered as temporal windows of opportunity, during which specific molecular steps could be targeted to prevent aberrant plasticity to develop.

Materials and methods

Key resources table

Reagent type (species) or resource	Designation	Source or reference	Identifiers	Additional information
Gene (*Mus musculus*)	Tor1a	MGI:1353568	Gene ID: 30931	official full name: torsin family 1, member A (torsin A)
Strain, strain background (*M. musculus*)	C57BL/6J mice	Charles River	catalog number B6JSIFE10SZ - C57BL/6J SPF/VAF; RRID:IMSR_JAX:000664	
Genetic reagent (*M. musculus*)	heterozygous knock-in Tor1a$^{+/\Delta gag}$	**Goodchild et al. (2005)**	-	maintained on the C57BL /6J background
Antibody	monoclonal anti-PSD-95	Neuromab	clone (k28/43) - catalog number 75–028; RRID:AB_2292909	dilution 1:2000 in I-Block
Antibody	monoclonal anti-GluN2B	Neuromab	clone 59/20 - catalog number 75–097; RRID:AB_10673405	dilution 1:1000 in I-Block
Antibody	polyclonal anti-GluA1	Merck Millipore	catalog number AB1504; RRID:AB_2113602	dilution 1:1000 in I-Block
Antibody	polyclonal anti-phospho -GluA1 (Ser845)	Merck Millipore	catalog number 04–1073; RRID:AB_1977219	dilution 1:1000 in I-Block
Antibody	polyclonal anti-GluN2A	Sigma-Aldrich	catalog number M264 RRID:AB_260485	dilution 1:1000 in I-Block
Antibody	monoclonal anti-GluA2	Neuromab	clone L21/32 - catalog number 75–002; RRID:AB_2232661	dilution 1:1000 in I-Block

Continued on next page

Continued

Reagent type (species) or resource	Designation	Source or reference	Identifiers	Additional information
Antibody	monoclonal anti-α-tubulin	Sigma-Aldrich	clone DM1A - catalog number T9026; RRID:AB_477593	dilution 1:5000 in I-Block
Antibody	goat anti-DARPP-32	R and D system	catalog number AF6259; RRID:AB_10641854	dilution 1:500 in I-Block
Antibody	mouse anti-Enkephalin	Millipore	catalog number MAB350; RRID:AB_2268028	dilution 1:1000 in I-Block
Antibody	mouse anti-β-actin	Sigma Aldrich	catalog number A5441; RRID:AB_476744	dilution 1:20000 in I-Block
Commercial assay or kit	Clarity Western ECL Substrate	BioRad	-	reagent used to visualize protein bands with Chemidoc Imaging System
Commercial assay or kit	ECL reagent	GEHealthcare	catalog number GERPN2232	reagent used to visualize protein bands with membranes were exposed to film
Commercial assay or kit	TRI-reagent	Sigma Aldrich	catalog number T9424	reagent used to RNA extraction
Commercial assay or kit	DNAase I	Invitrogen	catalog number AMPD1-1KT	reagent used for elimination of DNA from RNA
Commercial assay or kit	Transcriptor First Strand cDNA Synthesis Kit	Roche	catalog number 04379012001	reagent used to reverse transcribe RNA
Commercial assay or kit	Extract-N-Amp™ Tissue PCR Kit	SIGMA	catalog number XNAT2	genotyping primers UP- AGT CTG TGG CTG GCT CTC C; Low- CCT CAG GCTGCT CAC AAC C
Chemical compound, drug	ANA-12	Sigma-Aldrich	catalog number SML0209	in vivo administration
Chemical compound, drug	CNQX disodium salt	Tocris	catalog number 0190/10	application in bath during electrophysiology analysis
Chemical compound, drug	(+)-MK 801 maleate	Tocris	catalog number 0924/10	application in bath during electrophysiology analysis
Chemical compound, drug	Tetrodotoxin citrate (TTX)	Tocris	catalog number 1069/1	application in bath during electrophysiology analysis
Chemical compound, drug	Picrotoxin	Tocris	catalog number 1128/1	application in bath during electrophysiology analysis
Chemical compound, drug	Biocytin	Tocris	catalog number 3349/10	electrodes filled with biocytin, versatile marker used for neuroanatomical investigations of neuron IHC
Chemical compound, drug	Naspm trihydrochloride	Tocris	catalog number 2766/10	application in bath during electrophysiology analysis
Software, algorithm	ImageLab	BioRad	-	software used for quantification of protein bands in western blotting experiments
Software, algorithm	ImageJ software	NIH; ***Schneider et al. (2012)***	RRID:SCR_003070	software used for the quantification of protein bands in western blotting and confocal laser scanning microscope
Software, algorithm	ClampFit 9	pClamp	Molecular Devices; RRID:SCR_011323	data analysis
Software, algorithm	Origin 8.0	Microcal	RRID:SCR_002815	data analysis
Software, algorithm	Prism 5.3	GraphPad	RRID:SCR_002798	data analysis

Animal model

Studies were carried out in juvenile (P15-P35) and adult (P60-P75) knock-in *Tor1a*$^{+/\Delta gag}$ mice heterozygous for ΔE-torsinA, a mutation that removes a single glutamic acid residue (ΔE) from the torsinA protein, and in their wild-type *Tor1a*$^{+/+}$ littermates (**Goodchild et al., 2005**). Genotyping was performed as described (**Ponterio et al., 2018**). Animal breeding, on a C57Bl/6J background, and handling were performed in accordance with the guidelines for the use of animals in biomedical research provided by the European Union's directives and Italian laws (2010/63EU, D.lgs. 26/2014; 86/609/CEE, D.Lgs 116/1992). The experimental procedures were approved by Fondazione Santa Lucia and University Tor Vergata Animal Care and Use Committees, and the Italian Ministry of Health (authorization #223/2017-PR).

Experimental design

Age- and sex-matched wild-type and mutant littermates were randomly allocated to experimental groups. Investigators performing experiments and data analysis were blind to knowledge of genotype and treatment. Each observation was obtained from an independent biological sample. For electrophysiology, each cell was recorded from a different brain slice. All data were obtained from at least two animals in independent experiments. Biological replicates are represented with 'N' for number of animals and 'n' for number of cells. Sample size for any measurement was based on the ARRIVE recommendations on refinement and reduction of animal use in research, as well as on our previous studies.

Electrophysiology

Brain slice preparation

Mice were sacrificed by cervical dislocation, brains removed and sliced with a vibratome (Leica Microsystems) in oxygenated Krebs' solution (in mM: 126 NaCl, 2.5 KCl, 1.3 MgCl2, 1.2 NaH2PO4, 2.4 CaCl2, 10 glucose, 18 NaHCO3). Coronal and parasagittal corticostriatal slices (200–300 μm) were incubated in Krebs' solution at room temperature for 30 min. Then, individual slices were transferred into recording chambers continuously superfused with Krebs' solution (32–33°C) saturated with 95% O_2 and 5% CO_2.

Patch-clamp recordings

Recordings were performed with AxoPatch 200B amplifiers and pClamp 10.2 software (Molecular Devices). For voltage-clamp experiments, pipettes (2.5–5 MΩ) were filled with Cs^+ internal solution (in mM: 120 CsMeSO3, 15 CsCl, 8 NaCl, 10 TEA-Cl, 10 HEPES, 0.2 EGTA, 2 Mg-ATP, and 0.3 Na-GTP; pH 7.3 adjusted with CsOH; 300 mOsm). For whole-cell recordings of glutamatergic sEPSCs, SPNs were clamped at HP=−70 mV in the presence of the $GABA_A$ receptor antagonist PTX (50 μM). For GABAergic sIPSCs, SPNs were recorded at HP =+ 10 mV in MK801 (30 μM) and CNQX (10 μM) to block NMDARs and AMPARs, respectively. Both mEPSCs and mIPSCs were measured by adding 1 μM TTX. PPR was measured at HP=−70 mV in PTX by delivering two stimuli at 25–1000 ms ISI. Synaptic strength was analyzed by measuring the NMDAR/AMPAR ratio at HP =+ 40 mV in PTX. The AMPAR–mediated component of EPSC was isolated in MK-801 and the NMDAR component was obtained by digital subtraction of the AMPAR component from the dual-component EPSC (**Sciamanna et al., 2012**). The AMPAR and NMDAR IV relationships were measured in the presence of PTX *plus* MK-801 or CNQX, respectively. The RI was calculated as ratio of the mean EPSC amplitudes measured at +40 mV and −70 mV.

Sharp-electrode recordings

Current-clamp recordings of SPNs were performed with intracellular electrodes filled with 2M KCl (30–60 MΩ). Corticostriatal EPSPs were recorded in PTX (50 μM). HFS (three trains 100 Hz, 3 s, 20 s apart) was delivered at suprathreshold intensity to induce LTD. Magnesium was omitted to optimize LTP induction (**Calabresi et al., 1992b**). The EPSP amplitude was averaged and plotted over-time as percentage of control pre-HFS amplitude.

Gene expression analysis

P26 *Tor1a*$^{+/+}$ and *Tor1a*$^{+/\Delta gag}$ mouse cortex was collected in PCR clean tubes and stored at −80˚C. Total RNA was isolated using TRI-reagent (Sigma Aldrich), quantified and treated with DNAase I (Invitrogen). Integrity was confirmed by 1% agarose gel electrophoresis. RNA was reverse-transcribed using random hexamer primer and anchored-oligo (dT)18 primer according to the manufacturer's instructions (Transcriptor First Strand cDNA Synthesis Kit, Roche). Real-time PCR was performed on 25 ng cDNA by using LightCycler 480 Probes Master (04707494001, Roche) with Roche Light Cycler LC480 system, Bdnf and Hprt1 primers designed on the Roche Universal Probe Library Assay Design Center: https://configurator.realtimeready.roche.com/assaysupply_cp/pages/singleAssays/searchResult.jsf

Raw Ct values for Bdnf gene were normalized to the endogenous control gene Hprt1. Technical triplicates were analyzed for all samples and mean values were utilized for statistical analysis. The relative expression was determined using the $2^{-\Delta\Delta Ct}$ method (***Livak and Schmittgen, 2001***).

Immunohistochemistry

To identify direct- and indirect-pathway SPNs electrodes were loaded with biocytin, as described (***Martella et al., 2009***). Briefly, slices were fixed with 4% PFA in 0.12 M PB and 30 µm thick sections were cut from each slice with a freezing microtome, then dehydrated with serial alcohol dilutions to improve antigen retrieval and reduce background (***Buchwalow et al., 2011***). We used the following primary antibodies: goat anti-DARPP-32 (1:500 AF6259, R and D system), mouse anti-Enkephalin (1:1000 MAB350, Millipore), and secondary antibodies: anti-goat alexa 647 (Invitrogen), anti-mouse cyanine 3 (Jackson ImmunoResearch) and streptavidin-conjugated alexa 488 (Life Technologies). All sections used for analysis were processed together. Images were acquired with a LSM700 Zeiss confocal laser scanning microscope and analyzed with ImageJ software (NIH; ***Schneider et al., 2012***). Noise was reduced by applying background subtraction in ImageJ.

Subcellular fractionation and western blotting (WB)

To obtain a preparation that contains selectively proteins of the post-synaptic density (PSD), subcellular fractionation of striatal tissue was performed as reported (***Gardoni et al., 2006***; ***Paillé et al., 2010***) with minor modifications. Briefly, striata were homogenized with a Teflon-glass potter in ice-cold 0.32M sucrose containing 1 mM HEPES pH 7.4, 1 mM $MgCl_2$,1mM EDTA, 1 mM $NaHCO_3$, 0.1 mM phenylmethanesulfonylfluoride (PMSF) in the presence of a complete set of proteases and phosphatase inhibitors (Complete™ Protease Inhibitor Cocktail Tablets and PhosSTOP™ Phosphatase Inhibitor Cocktail, Roche Diagnostics). The homogenized tissue was centrifuged at 13,000 g for 15 min. The pellet was re-suspended in a buffer containing 75 mM KCl and 1% Triton X-100 and spun at 100,000 g for 1 hr. The final pellet, referred to as Triton-insoluble postsynaptic fraction (TIF), was homogenized in a glass-glass potter in 20 mM HEPES supplemented with Complete™ tablets and stored at −80˚C until use. Protein samples were separated onto an acrylamide/bisacrylamide gel at the appropriate concentration, transferred to a nitrocellulose membrane and immunoblotted with the appropriate primary and HRP-conjugated secondary antibodies. For WB analysis, the following unconjugated primary antibodies were used: polyclonal anti-GluN2A antibody (Sigma-Aldrich); monoclonal anti-GluN2B antibody (NeuroMab); polyclonal anti-GluA1 antibody (Merck Millipore); polyclonal anti-phospho-GluA1 (Ser845; Merck Millipore); monoclonal anti-GluA2 antibody (NeuroMab); monoclonal anti-PSD-95 antibody (NeuroMab); monoclonal anti-α-tubulin antibody (Sigma-Aldrich). Membrane development was performed with the reagent Clarity Western ECL Substrate (Bio-Rad) and labeling was visualized by Chemidoc Imaging System and ImageLab software (Bio-Rad). For quantification, each protein was normalized against the corresponding α-tubulin band.

WB analysis of BDNF on mouse striatum was performed as described (***Sciamanna et al., 2015***; ***Ponterio et al., 2018***). Protein extracts (15–30 µg) were loaded with page LDS sample buffer (Invitrogen, Waltham, Massachusetts, USA) containing DTT and denatured at 95˚C for 5 min. Proteins were separated on 15% SDS-PAGE, and transferred onto 0.45 µm polyvinylidene fluoride (PVDF) membranes. The following primary antibodies were utilized: rabbit anti-BDNF (1:200 sc-546, SantaCruz Biotechnology) and mouse anti-β-actin (1:20.000 A5441, Sigma Aldrich), as loading control, followed by anti-rabbit or anti-mouse horseradish peroxidase (HRP)-conjugated secondary antibodies. Immunodetection was performed by ECL reagent (GEHealthcare) and membranes were

exposed to film (Amersham). Quantification of the band intensity on scanned filters was achieved by ImageJ software.

Spine morphology

Carbocyanine dye DiI (Invitrogen) was used to label neurons as previously described (***Kim et al., 2007***; ***Stanic et al., 2015***). Images were taken using an inverted LSM510 confocal microscope (Zeiss). For morphological analysis, cells were chosen randomly for quantification from four to eight different coverslips; images were acquired using the same settings/exposure times, and at least 10 cells for each condition were analyzed. Morphological analysis was performed with ImageJ software to measure spine density and size. For each dendritic spine the length, the head and neck width were measured, which was used to classify spines into categories (thin, stubby and mushroom) (***Harris et al., 1992***).

Statistical analysis

Data were analysed with ClampFit 9 (pClamp, Molecular Devices), Origin 8.0 (Microcal) and Prism 5.3 (GraphPad) softwares. All data were obtained from at least two independent experiments and are represented as mean ± SEM. Statistical significance was evaluated, as indicated in figure legends, using paired and unpaired Student's t test, and one-way ANOVA with post-hoc Tukey test and two-way ANOVA with Bonferroni posttest for group comparisons. Statistical tests were two-tailed, the confidence interval was 95%, and the alpha-level used to determine significance was set at $p<0.05$.

Acknowledgements

We wish to thank Dystonia Medical Research Foundation for funding and for their work helping to increase understanding of this disease. Authors are grateful to Dr Nicole Calakos for critical reading of the manuscript and for helpful comments. We wish to thank also Elisa Zianni and Massimo Tolu for their skillful technical support. This work was supported by a PRIN 2010–2011 grant of the Ministero dell'Istruzione, dell'Università e della Ricerca to AP and FG.

Additional information

Funding

Funder	Grant reference number	Author
Ministero dell'Istruzione, dell'Università e della Ricerca	PRIN 2010-2011	Fabrizio Gardoni Antonio Pisani
Dystonia Medical Research Foundation	2017	Antonio Pisani

The funders had no role in study design, data collection and interpretation, or the decision to submit the work for publication.

Author contributions

Marta Maltese, Conceptualization, Data curation, Formal analysis, Investigation, Writing—original draft, Writing—review and editing; Jennifer Stanic, Data curation, Formal analysis, Investigation, Methodology, Writing—original draft; Annalisa Tassone, Paola Imbriani, Data curation, Formal analysis, Investigation, Methodology; Giuseppe Sciamanna, Data curation, Supervision, Investigation, Writing—review and editing; Giulia Ponterio, Data curation, Investigation, Methodology; Valentina Vanni, Investigation, Methodology; Giuseppina Martella, Formal analysis, Investigation, Methodology; Paola Bonsi, Fabrizio Gardoni, Conceptualization, Data curation, Writing—original draft, Writing—review and editing; Nicola Biagio Mercuri, Conceptualization, Supervision, Writing—review and editing; Antonio Pisani, Conceptualization, Data curation, Formal analysis, Supervision, Methodology, Writing—original draft, Writing—review and editing

Author ORCIDs
Giuseppina Martella http://orcid.org/0000-0002-8927-7107
Paola Imbriani https://orcid.org/0000-0003-3373-5073
Paola Bonsi http://orcid.org/0000-0001-5940-9028
Fabrizio Gardoni http://orcid.org/0000-0003-4598-5563
Antonio Pisani http://orcid.org/0000-0002-8432-594X

Ethics

Animal experimentation: Animal breeding and handling were performed in accordance with the guidelines for the use of animals in biomedical research provided by the European Union's directives and Italian laws (2010/63EU, D.lgs. 26/2014; 406 86/609/CEE, D.Lgs 116/1992). The experimental procedures were approved by Fondazione Santa Lucia and University Tor Vergata Animal Care and Use Committees and the Italian Ministry of Health (authorization #223/2017-PR).

Decision letter and Author response
Decision letter https://doi.org/10.7554/eLife.33331.018
Author response https://doi.org/10.7554/eLife.33331.019

Additional files

Supplementary files

- Transparent reporting form

DOI: https://doi.org/10.7554/eLife.33331.016

References

Altar CA, Cai N, Bliven T, Juhasz M, Conner JM, Acheson AL, Lindsay RM, Wiegand SJ. 1997. Anterograde transport of brain-derived neurotrophic factor and its role in the brain. *Nature* **389**:856–860. DOI: https://doi.org/10.1038/39885, PMID: 9349818

Baquet ZC, Gorski JA, Jones KR. 2004. Early striatal dendrite deficits followed by neuron loss with advanced age in the absence of anterograde cortical brain-derived neurotrophic factor. *Journal of Neuroscience* **24**:4250–4258. DOI: https://doi.org/10.1523/JNEUROSCI.3920-03.2004, PMID: 15115821

Bassani S, Folci A, Zapata J, Passafaro M. 2013. AMPAR trafficking in synapse maturation and plasticity. *Cellular and Molecular Life Sciences* **70**:4411–4430. DOI: https://doi.org/10.1007/s00018-013-1309-1, PMID: 23475111

Baydyuk M, Xu B. 2014. BDNF signaling and survival of striatal neurons. *Frontiers in Cellular Neuroscience* **8**:254. DOI: https://doi.org/10.3389/fncel.2014.00254, PMID: 25221473

Bellone C, Nicoll RA. 2007. Rapid bidirectional switching of synaptic NMDA receptors. *Neuron* **55**:779–785. DOI: https://doi.org/10.1016/j.neuron.2007.07.035, PMID: 17785184

Bhagat SL, Qiu S, Caffall ZF, Wan Y, Pan Y, Rodriguiz RM, Wetsel WC, Badea A, Hochgeschwender U, Calakos N. 2016. Mouse model of rare TOR1A variant found in sporadic focal dystonia impairs domains affected in DYT1 dystonia patients and animal models. *Neurobiology of Disease* **93**:137–145. DOI: https://doi.org/10.1016/j.nbd.2016.05.003, PMID: 27168150

Bressman SB, Sabatti C, Raymond D, de Leon D, Klein C, Kramer PL, Brin MF, Fahn S, Breakefield X, Ozelius LJ, Risch NJ. 2000. The DYT1 phenotype and guidelines for diagnostic testing. *Neurology* **54**:1746–1753. DOI: https://doi.org/10.1212/WNL.54.9.1746, PMID: 10802779

Buchwalow I, Samoilova V, Boecker W, Tiemann M. 2011. Non-specific binding of antibodies in immunohistochemistry: fallacies and facts. *Scientific Reports* **1**:28. DOI: https://doi.org/10.1038/srep00028, PMID: 22355547

Calabresi P, Maj R, Pisani A, Mercuri NB, Bernardi G. 1992a. Long-term synaptic depression in the striatum: physiological and pharmacological characterization. *The Journal of Neuroscience : The Official Journal of the Society for Neuroscience* **12**:4224–4233. PMID: 1359031

Calabresi P, Pisani A, Mercuri NB, Bernardi G. 1992b. Long-term potentiation in the striatum is unmasked by removing the voltage-dependent magnesium block of nmda receptor channels. *European Journal of Neuroscience* **4**:929–935. DOI: https://doi.org/10.1111/j.1460-9568.1992.tb00119.x, PMID: 12106428

Calabresi P, Pisani A, Rothwell J, Ghiglieri V, Obeso JA, Picconi B. 2016. Hyperkinetic disorders and loss of synaptic downscaling. *Nature Neuroscience* **19**:868–875. DOI: https://doi.org/10.1038/nn.4306, PMID: 27351172

Causing CG, Gloster A, Aloyz R, Bamji SX, Chang E, Fawcett J, Kuchel G, Miller FD. 1997. Synaptic innervation density is regulated by neuron-derived BDNF. *Neuron* **18**:257–267. DOI: https://doi.org/10.1016/S0896-6273(00)80266-4, PMID: 9052796

Cazorla M, Arrang JM, Prémont J. 2011. Pharmacological characterization of six trkB antibodies reveals a novel class of functional agents for the study of the BDNF receptor. *British Journal of Pharmacology* **162**:947–960. DOI: https://doi.org/10.1111/j.1476-5381.2010.01094.x, PMID: 21039416

Chen Q, Reiner A. 1996. Cellular distribution of the NMDA receptor NR2A/2B subunits in the rat striatum. *Brain Research* **743**:346–352. DOI: https://doi.org/10.1016/S0006-8993(96)01098-0, PMID: 9017267

Cull-Candy S, Kelly L, Farrant M. 2006. Regulation of Ca2+-permeable AMPA receptors: synaptic plasticity and beyond. *Current Opinion in Neurobiology* **16**:288–297. DOI: https://doi.org/10.1016/j.conb.2006.05.012, PMID: 16713244

Czöndör K, Thoumine O. 2013. Biophysical mechanisms regulating AMPA receptor accumulation at synapses. *Brain Research Bulletin* **93**:57–68. DOI: https://doi.org/10.1016/j.brainresbull.2012.11.001, PMID: 23174308

Dang MT, Yokoi F, Cheetham CC, Lu J, Vo V, Lovinger DM, Li Y. 2012. An anticholinergic reverses motor control and corticostriatal LTD deficits in Dyt1 ΔGAG knock-in mice. *Behavioural Brain Research* **226**:465–472. DOI: https://doi.org/10.1016/j.bbr.2011.10.002, PMID: 21995941

Dunah AW, Standaert DG. 2003. Subcellular segregation of distinct heteromeric NMDA glutamate receptors in the striatum. *Journal of Neurochemistry* **85**:935–943. DOI: https://doi.org/10.1046/j.1471-4159.2003.01744.x, PMID: 12716425

Edwards MJ, Huang YZ, Mir P, Rothwell JC, Bhatia KP. 2006. Abnormalities in motor cortical plasticity differentiate manifesting and nonmanifesting DYT1 carriers. *Movement Disorders* **21**:2181–2186. DOI: https://doi.org/10.1002/mds.21160, PMID: 17078060

Ehlers MD. 2000. Reinsertion or degradation of AMPA receptors determined by activity-dependent endocytic sorting. *Neuron* **28**:511–525. DOI: https://doi.org/10.1016/S0896-6273(00)00129-X, PMID: 11144360

Esteban JA, Shi SH, Wilson C, Nuriya M, Huganir RL, Malinow R. 2003. PKA phosphorylation of AMPA receptor subunits controls synaptic trafficking underlying plasticity. *Nature Neuroscience* **6**:136–143. DOI: https://doi.org/10.1038/nn997, PMID: 12536214

Flurkey K, Currer JM, Harrison DE. 2007. The Mouse in Aging Research. In: Fox J. G (Ed). *The Mouse in Biomedical Research*. 2nd Edition. Burlington: American College Laboratory Animal Medicine (Elsevier). p. 637–672.

Gardoni F, Picconi B, Ghiglieri V, Polli F, Bagetta V, Bernardi G, Cattabeni F, Di Luca M, Calabresi P. 2006. A critical interaction between NR2B and MAGUK in L-DOPA induced dyskinesia. *Journal of Neuroscience* **26**:2914–2922. DOI: https://doi.org/10.1523/JNEUROSCI.5326-05.2006, PMID: 16540568

Ghilardi MF, Carbon M, Silvestri G, Dhawan V, Tagliati M, Bressman S, Ghez C, Eidelberg D. 2003. Impaired sequence learning in carriers of the DYT1 dystonia mutation. *Annals of Neurology* **54**:102–109. DOI: https://doi.org/10.1002/ana.10610, PMID: 12838525

Gong LW, De Camilli P. 2008. Regulation of postsynaptic AMPA responses by synaptojanin 1. *PNAS* **105**:17561–17566. DOI: https://doi.org/10.1073/pnas.0809221105, PMID: 18987319

Goodchild RE, Grundmann K, Pisani A. 2013. New genetic insights highlight 'old' ideas on motor dysfunction in dystonia. *Trends in Neurosciences* **36**:717–725. DOI: https://doi.org/10.1016/j.tins.2013.09.003, PMID: 24144882

Goodchild RE, Kim CE, Dauer WT. 2005. Loss of the dystonia-associated protein torsinA selectively disrupts the neuronal nuclear envelope. *Neuron* **48**:923–932. DOI: https://doi.org/10.1016/j.neuron.2005.11.010, PMID: 16364897

Gray JA, Shi Y, Usui H, During MJ, Sakimura K, Nicoll RA. 2011. Distinct modes of AMPA receptor suppression at developing synapses by GluN2A and GluN2B: single-cell NMDA receptor subunit deletion in vivo. *Neuron* **71**:1085–1101. DOI: https://doi.org/10.1016/j.neuron.2011.08.007, PMID: 21943605

Grundmann K, Glöckle N, Martella G, Sciamanna G, Hauser TK, Yu L, Castaneda S, Pichler B, Fehrenbacher B, Schaller M, Nuscher B, Haass C, Hettich J, Yue Z, Nguyen HP, Pisani A, Riess O, Ott T. 2012. Generation of a novel rodent model for DYT1 dystonia. *Neurobiology of Disease* **47**:61–74. DOI: https://doi.org/10.1016/j.nbd.2012.03.024, PMID: 22472189

Harris KM, Jensen FE, Tsao B. 1992. Three-dimensional structure of dendritic spines and synapses in rat hippocampus (CA1) at postnatal day 15 and adult ages: implications for the maturation of synaptic physiology and long-term potentiation. *Journal of Neuroscience* **12**:2685–2705. PMID: 1613552

Hartog TE, Dittrich F, Pieneman AW, Jansen RF, Frankl-Vilches C, Lessmann V, Lilliehook C, Goldman SA, Gahr M. 2009. Brain-derived neurotrophic factor signaling in the HVC is required for testosterone-induced song of female canaries. *Journal of Neuroscience* **29**:15511–15519. DOI: https://doi.org/10.1523/JNEUROSCI.2564-09.2009, PMID: 20007475

Hensch TK. 2004. Critical period regulation. *Annual Review of Neuroscience* **27**:549–579. DOI: https://doi.org/10.1146/annurev.neuro.27.070203.144327, PMID: 15217343

Isaac JT, Ashby MC, McBain CJ. 2007. The role of the GluR2 subunit in AMPA receptor function and synaptic plasticity. *Neuron* **54**:859–871. DOI: https://doi.org/10.1016/j.neuron.2007.06.001, PMID: 17582328

Isaias IU, Alterman RL, Tagliati M. 2008. Outcome predictors of pallidal stimulation in patients with primary dystonia: the role of disease duration. *Brain* **131**:1895–1902. DOI: https://doi.org/10.1093/brain/awn120, PMID: 18567622

Jia Y, Gall CM, Lynch G. 2010. Presynaptic BDNF promotes postsynaptic long-term potentiation in the dorsal striatum. *Journal of Neuroscience* **30**:14440–14445. DOI: https://doi.org/10.1523/JNEUROSCI.3310-10.2010, PMID: 20980601

Johnston MV. 2004. Clinical disorders of brain plasticity. *Brain and Development* **26**:73–80. DOI: https://doi.org/10.1016/S0387-7604(03)00102-5, PMID: 15036425

Jourdi H, Iwakura Y, Narisawa-Saito M, Ibaraki K, Xiong H, Watanabe M, Hayashi Y, Takei N, Nawa H. 2003. Brain-derived neurotrophic factor signal enhances and maintains the expression of AMPA receptor-associated PDZ proteins in developing cortical neurons. *Developmental Biology* **263**:216–230. DOI: https://doi.org/10.1016/j.ydbio.2003.07.008, PMID: 14597197

Jourdi H, Kabbaj M. 2013. Acute BDNF treatment upregulates GluR1-SAP97 and GluR2-GRIP1 interactions: implications for sustained AMPA receptor expression. *PLoS One* **8**:e57124. DOI: https://doi.org/10.1371/journal.pone.0057124, PMID: 23460828

Kim BG, Dai HN, McAtee M, Vicini S, Bregman BS. 2007. Labeling of dendritic spines with the carbocyanine dye DiI for confocal microscopic imaging in lightly fixed cortical slices. *Journal of Neuroscience Methods* **162**:237–243. DOI: https://doi.org/10.1016/j.jneumeth.2007.01.016, PMID: 17346799

Kong H, Boulter J, Weber JL, Lai C, Chao MV. 2001. An evolutionarily conserved transmembrane protein that is a novel downstream target of neurotrophin and ephrin receptors. *Journal of Neuroscience* **21**:176–185. PMID: 11150334

Kopec CD, Real E, Kessels HW, Malinow R. 2007. GluR1 links structural and functional plasticity at excitatory synapses. *Journal of Neuroscience* **27**:13706–13718. DOI: https://doi.org/10.1523/JNEUROSCI.3503-07.2007, PMID: 18077682

Koshimizu H, Kiyosue K, Hara T, Hazama S, Suzuki S, Uegaki K, Nagappan G, Zaitsev E, Hirokawa T, Tatsu Y, Ogura A, Lu B, Kojima M. 2009. Multiple functions of precursor BDNF to CNS neurons: negative regulation of neurite growth, spine formation and cell survival. *Molecular Brain* **2**:27. DOI: https://doi.org/10.1186/1756-6606-2-27, PMID: 19674479

Krauss JK. 2002. Deep brain stimulation for dystonia in adults. Overview and developments. *Stereotactic and Functional Neurosurgery* **78**:168–182. DOI: https://doi.org/10.1159/000068963, PMID: 12652041

Ledoux MS, Dauer WT, Warner TT. 2013. Emerging common molecular pathways for primary dystonia. *Movement Disorders* **28**:968–981. DOI: https://doi.org/10.1002/mds.25547, PMID: 23893453

Lissin DV, Gomperts SN, Carroll RC, Christine CW, Kalman D, Kitamura M, Hardy S, Nicoll RA, Malenka RC, von Zastrow M. 1998. Activity differentially regulates the surface expression of synaptic AMPA and NMDA glutamate receptors. *PNAS* **95**:7097–7102. DOI: https://doi.org/10.1073/pnas.95.12.7097, PMID: 9618545

Livak KJ, Schmittgen TD. 2001. Analysis of relative gene expression data using real-time quantitative PCR and the 2(-Delta Delta C(T)) Method. *Methods* **25**:402–408. DOI: https://doi.org/10.1006/meth.2001.1262, PMID: 11846609

Malinverno M, Carta M, Epis R, Marcello E, Verpelli C, Cattabeni F, Sala C, Mulle C, Di Luca M, Gardoni F. 2010. Synaptic localization and activity of ADAM10 regulate excitatory synapses through N-cadherin cleavage. *Journal of Neuroscience* **30**:16343–16355. DOI: https://doi.org/10.1523/JNEUROSCI.1984-10.2010, PMID: 21123580

Maltese M, Martella G, Madeo G, Fagiolo I, Tassone A, Ponterio G, Sciamanna G, Burbaud P, Conn PJ, Bonsi P, Pisani A. 2014. Anticholinergic drugs rescue synaptic plasticity in DYT1 dystonia: role of M1 muscarinic receptors. *Movement Disorders* **29**:1655–1665. DOI: https://doi.org/10.1002/mds.26009, PMID: 25195914

Mandel AL, Ozdener H, Utermohlen V. 2009. Identification of pro- and mature brain-derived neurotrophic factor in human saliva. *Archives of Oral Biology* **54**:689–695. DOI: https://doi.org/10.1016/j.archoralbio.2009.04.005, PMID: 19467646

Martella G, Maltese M, Nisticò R, Schirinzi T, Madeo G, Sciamanna G, Ponterio G, Tassone A, Mandolesi G, Vanni V, Pignatelli M, Bonsi P, Pisani A. 2014. Regional specificity of synaptic plasticity deficits in a knock-in mouse model of DYT1 dystonia. *Neurobiology of Disease* **65**:124–132. DOI: https://doi.org/10.1016/j.nbd.2014.01.016, PMID: 24503369

Martella G, Tassone A, Sciamanna G, Platania P, Cuomo D, Viscomi MT, Bonsi P, Cacci E, Biagioni S, Usiello A, Bernardi G, Sharma N, Standaert DG, Pisani A. 2009. Impairment of bidirectional synaptic plasticity in the striatum of a mouse model of DYT1 dystonia: role of endogenous acetylcholine. *Brain* **132**:2336–2349. DOI: https://doi.org/10.1093/brain/awp194, PMID: 19641103

Mauceri D, Cattabeni F, Di Luca M, Gardoni F. 2004. Calcium/calmodulin-dependent protein kinase II phosphorylation drives synapse-associated protein 97 into spines. *Journal of Biological Chemistry* **279**:23813–23821. DOI: https://doi.org/10.1074/jbc.M402796200, PMID: 15044483

Mayer ML, Westbrook GL, Guthrie PB. 1984. Voltage-dependent block by Mg2+ of NMDA responses in spinal cord neurones. *Nature* **309**:261–263. DOI: https://doi.org/10.1038/309261a0, PMID: 6325946

McAllister AK, Katz LC, Lo DC, Dc L. 1997. Opposing roles for endogenous BDNF and NT-3 in regulating cortical dendritic growth. *Neuron* **18**:767–778. DOI: https://doi.org/10.1016/S0896-6273(00)80316-5, PMID: 9182801

Meredith RM. 2015. Sensitive and critical periods during neurotypical and aberrant neurodevelopment: a framework for neurodevelopmental disorders. *Neuroscience & Biobehavioral Reviews* **50**:180–188. DOI: https://doi.org/10.1016/j.neubiorev.2014.12.001, PMID: 25496903

Minichiello L, Korte M, Wolfer D, Kühn R, Unsicker K, Cestari V, Rossi-Arnaud C, Lipp HP, Bonhoeffer T, Klein R. 1999. Essential role for TrkB receptors in hippocampus-mediated learning. *Neuron* **24**:401–414. DOI: https://doi.org/10.1016/S0896-6273(00)80853-3, PMID: 10571233

Narisawa-Saito M, Carnahan J, Araki K, Yamaguchi T, Nawa H. 1999. Brain-derived neurotrophic factor regulates the expression of AMPA receptor proteins in neocortical neurons. *Neuroscience* **88**:1009–1014. DOI: https://doi.org/10.1016/S0306-4522(98)00496-5, PMID: 10336116

O'Brien RJ, Kamboj S, Ehlers MD, Rosen KR, Fischbach GD, Huganir RL. 1998. Activity-dependent modulation of synaptic AMPA receptor accumulation. *Neuron* **21**:1067–1078. DOI: https://doi.org/10.1016/S0896-6273(00)80624-8, PMID: 9856462

Oh MC, Derkach VA, Guire ES, Soderling TR. 2006. Extrasynaptic membrane trafficking regulated by GluR1 serine 845 phosphorylation primes AMPA receptors for long-term potentiation. *The Journal of Biological Chemistry* **281**:752–758. DOI: https://doi.org/10.1074/jbc.M509677200, PMID: 16272153

Ozelius LJ, Hewett JW, Page CE, Bressman SB, Kramer PL, Shalish C, de Leon D, Brin MF, Raymond D, Corey DP, Fahn S, Risch NJ, Buckler AJ, Gusella JF, Breakefield XO. 1997. The early-onset torsion dystonia gene (DYT1) encodes an ATP-binding protein. *Nature Genetics* **17**:40–48. DOI: https://doi.org/10.1038/ng0997-40, PMID: 9288096

Paillé V, Picconi B, Bagetta V, Ghiglieri V, Sgobio C, Di Filippo M, Viscomi MT, Giampà C, Fusco FR, Gardoni F, Bernardi G, Greengard P, Di Luca M, Calabresi P. 2010. Distinct levels of dopamine denervation differentially alter striatal synaptic plasticity and NMDA receptor subunit composition. *Journal of Neuroscience* **30**:14182–14193. DOI: https://doi.org/10.1523/JNEUROSCI.2149-10.2010, PMID: 20962239

Paoletti P, Bellone C, Zhou Q. 2013. NMDA receptor subunit diversity: impact on receptor properties, synaptic plasticity and disease. *Nature Reviews Neuroscience* **14**:383–400. DOI: https://doi.org/10.1038/nrn3504, PMID: 23686171

Pappas SS, Leventhal DK, Albin RL, Dauer WT. 2014. Mouse models of neurodevelopmental disease of the basal ganglia and associated circuits. *Current Topics in Developmental Biology* **109**:97–169. DOI: https://doi.org/10.1016/B978-0-12-397920-9.00001-9, PMID: 24947237

Partridge JG, Tang KC, Lovinger DM. 2000. Regional and postnatal heterogeneity of activity-dependent long-term changes in synaptic efficacy in the dorsal striatum. *Journal of Neurophysiology* **84**:1422–1429. DOI: https://doi.org/10.1152/jn.2000.84.3.1422, PMID: 10980015

Ponterio G, Tassone A, Sciamanna G, Vanni V, Meringolo M, Santoro M, Mercuri NB, Bonsi P, Pisani A. 2018. Enhanced mu opioid receptor-dependent opioidergic modulation of striatal cholinergic transmission in DYT1 dystonia. *Movement Disorders* **33**:310–320. DOI: https://doi.org/10.1002/mds.27212, PMID: 29150865

Quartarone A, Hallett M. 2013. Emerging concepts in the physiological basis of dystonia. *Movement Disorders* **28**:958–967. DOI: https://doi.org/10.1002/mds.25532, PMID: 23893452

Quartarone A, Rizzo V, Terranova C, Morgante F, Schneider S, Ibrahim N, Girlanda P, Bhatia KP, Rothwell JC. 2009. Abnormal sensorimotor plasticity in organic but not in psychogenic dystonia. *Brain* **132**:2871–2877. DOI: https://doi.org/10.1093/brain/awp213, PMID: 19690095

Rauskolb S, Zagrebelsky M, Dreznjak A, Deogracias R, Matsumoto T, Wiese S, Erne B, Sendtner M, Schaeren-Wiemers N, Korte M, Barde YA. 2010. Global deprivation of brain-derived neurotrophic factor in the CNS reveals an area-specific requirement for dendritic growth. *Journal of Neuroscience* **30**:1739–1749. DOI: https://doi.org/10.1523/JNEUROSCI.5100-09.2010, PMID: 20130183

Rittiner JE, Caffall ZF, Hernández-Martinez R, Sanderson SM, Pearson JL, Tsukayama KK, Liu AY, Xiao C, Tracy S, Shipman MK, Hickey P, Johnson J, Scott B, Stacy M, Saunders-Pullman R, Bressman S, Simonyan K, Sharma N, Ozelius LJ, Cirulli ET, et al. 2016. Functional genomic analyses of mendelian and sporadic disease identify impaired eif2α signaling as a generalizable mechanism for dystonia. *Neuron* **92**:1238–1251. DOI: https://doi.org/10.1016/j.neuron.2016.11.012, PMID: 27939583

Roche KW, O'Brien RJ, Mammen AL, Bernhardt J, Huganir RL. 1996. Characterization of multiple phosphorylation sites on the AMPA receptor GluR1 subunit. *Neuron* **16**:1179–1188. DOI: https://doi.org/10.1016/S0896-6273(00)80144-0, PMID: 8663994

Sanz-Clemente A, Nicoll RA, Roche KW. 2013. Diversity in NMDA receptor composition: many regulators, many consequences. *The Neuroscientist* **19**:62–75. DOI: https://doi.org/10.1177/1073858411435129, PMID: 22343826

Schneider CA, Rasband WS, Eliceiri KW. 2012. NIH Image to ImageJ: 25 years of image analysis. *Nature Methods* **9**:671–675. DOI: https://doi.org/10.1038/nmeth.2089, PMID: 22930834

Sciamanna G, Napolitano F, Pelosi B, Bonsi P, Vitucci D, Nuzzo T, Punzo D, Ghiglieri V, Ponterio G, Pasqualetti M, Pisani A, Usiello A. 2015. Rhes regulates dopamine D2 receptor transmission in striatal cholinergic interneurons. *Neurobiology of Disease* **78**:146–161. DOI: https://doi.org/10.1016/j.nbd.2015.03.021, PMID: 25818655

Sciamanna G, Tassone A, Mandolesi G, Puglisi F, Ponterio G, Martella G, Madeo G, Bernardi G, Standaert DG, Bonsi P, Pisani A. 2012. Cholinergic dysfunction alters synaptic integration between thalamostriatal and corticostriatal inputs in DYT1 dystonia. *Journal of Neuroscience* **32**:11991–12004. DOI: https://doi.org/10.1523/JNEUROSCI.0041-12.2012, PMID: 22933784

Stanic J, Carta M, Eberini I, Pelucchi S, Marcello E, Genazzani AA, Racca C, Mulle C, Di Luca M, Gardoni F. 2015. Rabphilin 3A retains NMDA receptors at synaptic sites through interaction with GluN2A/PSD-95 complex. *Nature Communications* **6**:10181. DOI: https://doi.org/10.1038/ncomms10181, PMID: 26679993

Stragier E, Martin V, Davenas E, Poilbout C, Mongeau R, Corradetti R, Lanfumey L. 2015. Brain plasticity and cognitive functions after ethanol consumption in C57BL/6J mice. *Translational Psychiatry* **5**:e696. DOI: https://doi.org/10.1038/tp.2015.183, PMID: 26670281

Tropea TF, Kabir ZD, Kaur G, Rajadhyaksha AM, Kosofsky BE. 2011. Enhanced dopamine D1 and BDNF signaling in the adult dorsal striatum but not nucleus accumbens of prenatal cocaine treated mice. *Frontiers in Psychiatry* **2**:67. DOI: https://doi.org/10.3389/fpsyt.2011.00067, PMID: 22162970

Turrigiano GG, Nelson SB. 2004. Homeostatic plasticity in the developing nervous system. *Nature Reviews Neuroscience* **5**:97–107. DOI: https://doi.org/10.1038/nrn1327, PMID: 14735113

Vercueil L, Pollak P, Fraix V, Caputo E, Moro E, Benazzouz A, Xie J, Koudsie A, Benabid AL. 2001. Deep brain stimulation in the treatment of severe dystonia. *Journal of Neurology* **248**:695–700. DOI: https://doi.org/10.1007/s004150170116, PMID: 11569899

Vidailhet M, Pollak P. 2005. Deep brain stimulation for dystonia: make the lame walk. *Annals of Neurology* **57**: 613–614. DOI: https://doi.org/10.1002/ana.20491, PMID: 15852405

Weise D, Schramm A, Stefan K, Wolters A, Reiners K, Naumann M, Classen J. 2006. The two sides of associative plasticity in writer's cramp. *Brain* **129**:2709–2721. DOI: https://doi.org/10.1093/brain/awl221, PMID: 16921180

Wichmann T, Delong MR. 2006. Deep brain stimulation for neurologic and neuropsychiatric disorders. *Neuron* **52**:197–204. DOI: https://doi.org/10.1016/j.neuron.2006.09.022, PMID: 17015236

Zermeño V, Espindola S, Mendoza E, Hernández-Echeagaray E. 2009. Differential expression of neurotrophins in postnatal C57BL/6 mice striatum. *International Journal of Biological Sciences* **5**:118–127. DOI: https://doi.org/10.7150/ijbs.5.118, PMID: 19173033